The Transition to a Subtropical Jet Regime and Its Maintenance

ORLI LACHMY AND NILI HARNIK

Tel-Aviv University, Tel-Aviv, Israel

ABSTRACT

An abrupt transition from a merged jet regime to a subtropical jet regime is analyzed using a two-layer modified quasigeostrophic (QG) spherical model. Unlike the common version of QG models, this model includes advection of the zonal mean momentum by the ageostrophic mean meridional circulation, allowing for a relatively realistic momentum balance in the tropics and subtropics. The merged jet is a single jet inside the Ferrel cell created by a merging of the subtropical and eddy-driven jets, and the subtropical jet is a mainly thermally driven jet at the Hadley cell edge. The maintenance of each type of jet depends on the dominant baroclinic modes. In the merged jet regime, the spectrum is dominated by intermediate-scale (wavenumbers 4–6) fast waves at the midlatitudes that grow close to the jet maximum. In the subtropical jet regime, the spectrum is dominated by long (wavenumbers 1–3) slow westward-propagating waves at high latitudes and somewhat weaker intermediate-scale slow waves at the midlatitudes. In the subtropical jet regime, waves equilibrate at weaker amplitudes than in the merged jet regime. A mechanism is found that explains why baroclinic instability is weaker in the subtropical jet regime, although the vertical shear of the mean flow is stronger, which has to do with the lower-level potential vorticity (PV) structure. The relevance of these results to the real atmosphere seams to hold in local zonal sections but not for the zonal mean.

1. Introduction

One of the most prominent features of the zonal mean flow in the atmosphere is the upper-tropospheric jet, which is a local maximum of the zonal wind. Two different processes may be responsible for creating jets in the atmosphere: one is advection of planetary angular momentum by the mean meridional circulation (MMC) and the other is convergence of eddy momentum flux (Lee and Kim 2003). Since the MMC in the tropics is driven mainly by thermal processes, the term "thermally driven jet" has been used to describe a jet created by the MMC, while jets created by eddy momentum flux convergence (EMFC) were referred to as "eddy-driven jets."

Theoretically, a purely thermally driven jet may exist only in an axisymmetric model with no eddies (Held and Hou 1980), while a pure eddy-driven jet may exist in the absence of advection of planetary momentum—for example, in a turbulent model with latitudinally uniform baroclinic forcing (Panetta 1993). Each process would create a jet with different properties. In the troposphere, a thermally driven jet would be located at the subtropical edge of the Hadley cell, while an eddy-driven jet would be located inside the Ferrel cell where the EMFC is strongest. Since surface westerlies exist at the lower branch of the Ferrel cell, where the Coriolis force maintains them against the surface friction, the eddy-driven jet would continue from the upper troposphere to the surface, while below the thermally driven jet the surface wind would be close to zero, since there is no Coriolis force to balance the friction. It is expected that the location and structure of the jet would be an indication for the main mechanism creating the jet.

In the upper troposphere, a jet with a strong vertical shear that is located at the Hadley cell edge dominates the climatology of the zonal mean flow during winter in both hemispheres (Fig. 1) and is often referred to as a "subtropical jet." There is a state where both a subtropical jet at the edge of the Hadley cell and an eddy-driven jet inside the Ferrel cell are present. This double jet state is seen, for example, above the North Atlantic (Eichelberger and Hartmann 2007) and in the Southern Hemisphere equinox. There is a state where a single jet is seen inside the Ferrel cell, as in the Southern Hemisphere summer

Corresponding author address: Orli Lachmy, Department of Geophysical, Atmospheric and Planetary Sciences, Tel Aviv University, Tel-Aviv 69978, Israel.
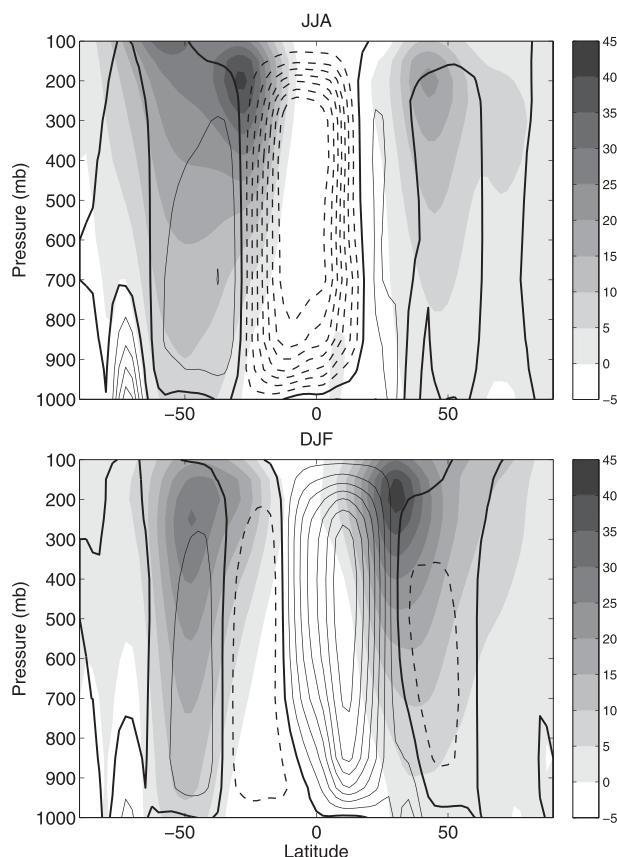E-mail: orlipast@post.tau.ac.il

FIG. 1. Climatology of the zonal mean zonal wind (shading, m s^{-1}) and meridional streamfunction (contours) as a function of pressure and latitude for (top) the NH summer/SH winter (JJA) and (bottom) NH winter/SH summer (DJF), based on the National Centers for Environmental Prediction–National Center for Atmospheric Research (NCEP–NCAR) reanalysis data for years 1969–2011. Thin solid, dashed, and thick solid contours are for positive, negative, and zero values of the streamfunction, respectively, with a contour interval 2×10^{10} kg s^{-1}.

(Fig. 1) and above the North Pacific (Eichelberger and Hartmann 2007). This type of jet is sometimes viewed as a single eddy-driven jet or a merged (subtropical and eddy driven) jet. The term "merged" is justified by numerical studies showing merging of the two types of jets (Kim and Lee 2004; Son and Lee 2005; O'Rourke and Vallis 2013). In this paper, we shall focus on two regimes: one with a single jet at the edge of the Hadley cell, which we refer to as "subtropical," and the other with a single jet inside the Ferrel cell, which we refer to as merged.

A theory for the existence of the different types of jets in the atmosphere should explain how the interactions between the zonal mean zonal momentum, the MMC, and the eddies maintain each state in balance. The maintenance of the merged jet is relatively well understood (Robinson 2006; Gerber and Vallis 2007). Baroclinic

eddies growing in the midlatitudes propagate meridionally in the upper troposphere. According to the Eliassen–Palm (EP) flux theorem, this meridional propagation is accompanied by a transfer of westerly momentum into the source region (Salmon et al. 2001), creating a barotropic jet in the midlatitudes. The baroclinicity of this jet is restored by surface friction and thermal driving, enabling waves to keep growing at the same latitude and maintain the jet by their momentum flux (Robinson 2006).

The maintenance of the subtropical jet in the presence of baroclinic eddies, however, is less clear. An analysis of the zonal momentum balance shows why this is not trivial. The zonal momentum budget in the upper troposphere is close to satisfying the following equation for the zonal mean momentum in steady state (Dima et al. 2005):

$$\left\{ f - \frac{1}{a\cos(\phi)} \frac{\partial[\cos(\phi)\overline{u}]}{\partial\phi} \right\} \cdot \overline{v}$$
$$= \frac{1}{a\cos^2(\phi)} \frac{\partial}{\partial\phi} [\cos^2(\phi) \cdot \overline{(u'v')}], \qquad (1)$$

where f is the Coriolis parameter; a is Earth's radius; u and v are the zonal and meridional winds, respectively; and ϕ is the latitude. The overbar denotes zonal averaging and the prime denotes deviation from the zonal average (i.e., eddy component). An interesting outcome of Eq. (1) is that the EMFC (minus the rhs term) has to change sign where the meridional wind is zero [i.e., at the edges of the circulation cells (Korty and Schneider 2008)]. In the climatology of the seasonal cycle in the upper troposphere, the EMFC is always negative inside the Hadley cell and positive inside the Ferrel cell (Son and Lee 2005). This means that a subtropical jet at the Hadley cell edge is necessarily located where the EMFC is zero and that waves constantly try to displace it poleward, while the Coriolis force does the opposite. To the extent that the EP flux is nondivergent, the latitude of maximum EMFC is close to the latitude of maximum poleward heat flux and baroclinic growth, so that in a balanced state with a subtropical jet, baroclinic waves necessarily grow poleward of the jet latitude, as observed in the winter climatology of both hemispheres (Randel and Held 1991; Kim and Lee 2004). Two questions arise concerning the maintenance of the subtropical jet: Why does the jet remain at the edge of the Hadley cell rather than being displaced poleward into the Ferrel cell by eddy momentum fluxes? Why does the baroclinic growth occur far poleward of the jet latitude even though the subtropical jet has a strong vertical shear?

The poleward shift of the baroclinic growth relative to the subtropical jet may be attributed to the properties of the linear instability of the jet. Lee and Kim (2003) have

shown in a numerical study that for a relatively weak subtropical jet (with a peak of about $40\,\mathrm{m\,s^{-1}}$) linear baroclinic instability occurs about 25° poleward of the jet, while for a strong jet ($50\,\mathrm{m\,s^{-1}}$ or higher) instability occurs below the jet. The latter case raises the question how subtropical jets with a peak of more than $50\,\mathrm{m\,s^{-1}}$ are maintained in the atmosphere, since as explained above, it is not possible to maintain a jet at the edge of the Hadley cell in a steady state with baroclinic growth at the latitude of the jet. Nakamura et al. (2004) suggest that the poleward shift of the baroclinic growth region relative to the latitude of the subtropical jet is due to a strong surface temperature gradient in the midlatitudes, which is maintained by a feedback between the surface westerlies and the midlatitude oceanic front. This reasoning however does not explain why this poleward shift is found also in numerical models of the atmosphere, which do not include interaction with the ocean (Lee and Kim 2003; Kim and Lee 2004; Robinson 2006).

Analysis of an atmospheric model in a steady state with a subtropical jet may add to the understanding of the maintenance of this type of jet. While many aquaplanet atmospheric GCMs are able to reproduce a steady state with a single jet inside the Ferrel cell or a state with a double jet (e.g., Son and Lee 2005; Gerber and Vallis 2007; Eichelberger and Hartmann 2007), a steady state with a single jet that peaks at the edge of the Hadley cell is more difficult to achieve in such a model (S. Feldstein 2013, personal communication). It is possible to reproduce a steady state with a subtropical jet when the model is forced by radiative damping to an empirical profile (Kim and Lee 2004) or in a state with an unrealistically weak jet (Robinson 2006). However, we have not found a paper discussing the maintenance of a realistically strong subtropical jet in a model without empirical forcing.

In the present study, we explore the dynamics responsible for the maintenance of the subtropical and merged jet regimes and the transition between them. The transition between these two regimes may be abrupt as the external forcing is varied (Robinson 2006), indicating that a positive feedback in the internal dynamics of the system may be present. The role of the wave energy in this feedback is studied by gradually changing the static stability and the wave damping. The external forcing is varied as well in order to compare with previous studies and observations. The model was designed to contain only the minimal components necessary for qualitatively reproducing the characteristics of the zonal mean flow in the troposphere.

A description of the model is given in section 2. Section 3 shows the transition in the type of jet found in a parameter sweep of the model and discusses the mechanism of the transition. In section 4, the spectral properties of the waves in each flow regime are analyzed and compared with Southern Hemisphere observations. Section 5 discusses the results of a parameter sweep in which the tropical diabatic heating was varied and compares it with observational and numerical studies in the literature, revealing the relevance of the mechanisms found in the model to the atmospheric flow. The results are summarized section 6.

2. Model description

The numerical model was chosen to include the minimal components necessary for capturing the dynamics of the jet type transition. These include the interaction between the zonal mean zonal wind, the MMC, and the waves, which we will sometimes refer to as "eddies," defined as deviations from the zonal mean. Radiative damping to an equilibrium profile and surface friction are also introduced to allow for a balanced state of the heat and momentum budget. The model has two layers in the vertical direction, representing the upper and lower troposphere and allowing for both baroclinic and barotropic processes. The waves are treated separately from the zonal mean flow to allow for the use of slightly different assumptions and to aid the conceptual separation between them. The nonlinear wave–wave terms are retained in the equations for the waves and for the mean flow. Hyperdiffusion removes the energy from the smallest scales.

The model equations are a version of the quasigeostrophic (QG) equations on a sphere, but without neglecting the ageostrophic term representing the advection of zonal mean momentum by the MMC. This somewhat unusual set of approximations allows for a qualitatively realistic zonal mean momentum balance while retaining the simplicity of the QG framework. An elaborate derivation and justification of the model equations is given in appendixes A and B. The model equations are a two-layer version of the following equations: (i) the zonal mean zonal geostrophic wind equation with the ageostrophic advection terms and surface friction included, (ii) the wave potential vorticity (PV) equation with surface friction and radiative relaxation to zero temperature anomaly, and (iii) a diagnostic equation for the ageostrophic zonal mean meridional wind. The first two are given by

$$\frac{\partial \overline{U_g}}{\partial t} = \left(2\Omega\mu - \frac{1}{a}\frac{\partial \overline{U_g}}{\partial \mu}\right)\overline{V_a} - \frac{\partial \overline{U_g}}{\partial z}\overline{w_a}$$
$$- \frac{1}{a}\frac{\partial \overline{(U_g'V_g')}}{\partial \mu} - \frac{\overline{U_g}}{\tau_f}\delta(z) \quad \text{and} \tag{2}$$

$$\frac{\partial q'}{\partial t} = -\frac{\overline{U_g}}{a(1-\mu^2)}\frac{\partial q'}{\partial \lambda} - \frac{V'_g}{a}\frac{\partial \overline{q}}{\partial \mu} - \left[\frac{U'_g}{a(1-\mu^2)}\frac{\partial q'}{\partial \lambda}\right]'$$

$$- \left(\frac{V'_g}{a}\frac{\partial q'}{\partial \mu}\right)' - \frac{\nabla^2 \psi'}{\tau_f}\delta(z) - \frac{1}{\tau_r}\left(\frac{2\Omega\mu}{N}\right)^2\frac{\partial^2 \psi'}{\partial z^2}, \quad (3)$$

where $U \equiv u\cos\phi$; $V \equiv v\cos\phi$; $\mu \equiv \sin\phi$; subscripts g and a denote the geostrophic and ageostrophic components, respectively; q is PV; ψ is the streamfunction from which U_g and V_g are derived [see Eqs. (A5a), (A5b)]; ∇^2 is the spherical horizontal Laplacian operator; λ is the longitude in radians; and Ω, a, τ_f, and τ_r are Earth's rotation rate, Earth's radius, the surface friction time scale, and the radiative damping time scale, respectively. The relation between q' and ψ' is given by the perturbation from the zonal mean of Eq. (A1). The full two-layer model equations [Eqs. (A7a), (A7b), (A9), (A10a), (A10b)] and their derivation are given in appendix A. The two layers have equal thickness and the variables at the upper and lower layers are taken at the middle of each layer and denoted by subscripts 1 and 2, respectively.

The equations depend on several parameters. The following parameters were fixed in all the model integrations: $a = 6370$ km, $\Omega = 7.3 \times 10^{-5}$ s^{-1}, the Brunt–Väisälä frequency $N = 10^{-2}$ s^{-1}, and numerical diffusion coefficient ν. The parameters τ_f, τ_r, and $\epsilon \equiv 8(a\Omega/NH)^2$ were varied between the model integrations, where ϵ was varied by changing H, which is the thickness of each layer of the model. Note that H and N appear in the equations only through ϵ; therefore increasing H is equivalent to increasing N (i.e., increasing the static stability). The numerical diffusion coefficient was given different values for the mean flow and the waves owing to the different typical length scales. In all the integrations presented in this paper the numerical diffusion coefficients were $(\nu)_{MF} = 4 \times 10^{14}$ m^4 s^{-1} for the mean flow and $(\nu)_{WV} = 6 \times 10^{16}$ m^4 s^{-1} for the waves. Those are the minimal values needed to prevent the accumulation of energy in the smallest scales. Also τ_f and τ_r were given different values for the mean flow and the waves in order to examine the role of the wave energy. The damping time scales for the mean flow were the same for all integrations: $[(\tau_r)_{MF}]^{-1} = 10^{-6}$ s^{-1}, which is equivalent to a radiative damping time scale of about 11.6 days, and $[(\tau_r)_{MF}]^{-1} = 3 \times 10^{-6}$ s^{-1}, which gives a surface friction time scale of about 3.9 days. The wave damping time scales $(\tau_f)_{WV}$ and $(\tau_r)_{WV}$ were varied between the model integrations by changing a wave damping parameter, r, such that $1/(\tau_f)_{WV} = r/(\tau_f)_{MF}$ and $1/(\tau_r)_{WV} = r/(\tau_r)_{MF}$. Note that larger values of r correspond to stronger wave damping. One set of integrations includes additional tropical diabatic heating, as explained in section Ac. The intensity of the heating is controlled by a parameter D (defined in section Ac).

The radiative equilibrium profile of the thermal wind $(\overline{U_T})_E(\phi)$ was the same in all model integrations presented in this paper:

$$(\overline{U_T})_E(\phi)$$
$$= \begin{cases} (U_T)_0 \cos\phi \cot\phi(\sin\phi - \sin\phi_0) & \text{for} \quad |\phi| > \phi_0 \\ (\overline{U_T})_E(\phi) = 0 & \text{for} \quad |\phi| \leq \phi_0 \end{cases},$$
$$(4)$$

where $\overline{U_T}$ is defined as half the difference between $\overline{U}$ in the two layers, $(U_T)_0 = 15$ m s^{-1}, $\phi_0 = 10°$. This profile is based on the radiative equilibrium temperature profile of Lindzen and Hou (1988), which satisfies $\theta_e \propto (\sin\phi - \sin\phi_0)^2$. Using the thermal wind relations, $(\sin\phi)(\partial u/\partial z) \propto \partial\theta/\partial\phi$ gives $u_T \propto \cot\phi(\sin\phi - \sin\phi_0)$. This profile causes the Hadley cell ascending branch to be concentrated around ϕ_0 and is meant to simulate winter conditions for the Southern Hemisphere. We focus in this paper only on winter conditions, where we found a clear transition between a merged and a subtropical jet regime.

Three sets of model integrations were conducted (Table 1), and in each one a different parameter was varied: In set H, the layer thickness H was varied in order to control the energy of the waves while keeping the same damping parameters for the waves and the mean flow—as H is increased, the vertical shear is decreased for a given $\overline{u_1}$ and $\overline{u_2}$ and the flow becomes less baroclinically unstable. The layer thickness appears not only in the vertical shear of the mean flow, but in every term in the equations that includes a vertical derivative—for example, the stretching term in the definition of the PV [last term on the rhs of Eq. (A1)]—thus increasing H increases the role of barotropic processes relative to baroclinic processes. In set r, the wave damping parameter r is varied to show the similarity to set H and emphasize the role of the wave amplitude in the transition that appears as H is varied. In set D, the tropical diabatic heating parameter D is varied in order to test the role of external forcing in determining the flow regime.

All model integrations had the same initial conditions. The initial conditions for both the mean and the waves were taken from day 175 of an integration that was initiated by a Gaussian meridional profile for the upper-layer zonal mean wind $\overline{U_1}$ with zero surface winds and a small-amplitude wavenumber-6 disturbance with a Gaussian profile of $\overline{|q'_1|}$ and $\overline{|q'_2|}$. These conditions were used in order to save time for the adjustment of the system to steady state. We assume insensitivity of the final

TABLE 1. The sets of parameter sweeps.

Set	Parameter	Values	Values of constant parameters
H	H (km)	7, 7.5, 8, 8.5, 8.8, 9, 9.2, 9.5, 9.6, 9.7, 9.8, 10, 10.2, 10.5, 11	$r = 1$, $D = 0$
r	r (Dimensionless wave damping parameter)	0.2, 0.5, 0.7, 0.8, 1, 1.2, 1.5, 1.8, 2, 2.5, 3	$H = 9.5$ km, $D = 0$
D	D (Dimensionless diabatic heating parameter)	0, 0.2, 0.35, 0.5, 0.65, 0.8, 1, 1.5, 2	$H = 10$ km, $r = 1$

steady state to initial conditions and a few tests support this. All integrations were conducted for 1500 model days and then averaged over a statistically steady-state period, which was the last 1000 days for most integrations, except for those near the jet-type transition line, for which equilibration took longer and will be mentioned explicitly in the text.

3. A jet-type transition

From the three sets of parameter sweeps described in Table 1, it was found that the properties of the statistically steady-state mean-flow change abruptly as the parameters H, r, or D each reach a critical value. Figure 2 shows the upper-layer mean zonal wind $\overline{u_1}$ and the baroclinic mean meridional wind $\overline{v_T}$ [obtained from Eq. (A9)] as a function of latitude and parameter (Figs. 2a,b) and the lower-layer mean zonal wind $\overline{u_2}$ and $\overline{v_T}$ (Figs. 2c,d) for sets H and r. (The same variables for set D are shown in Fig. 8 and discussed separately in section 5.) All variables are time averages over the statistically steady-state period, which is from days 500 to 1500 for all integrations, except for $H = 9.7$ and $H = 9.8$ from set H, for which the statistically steady averaging period is from days 1200 to 1500 and days 800 to 1500, respectively.

It is seen from Figs. 2a–d that for $H \leq 9.6$ in set H and $r \leq 1$ in set r the upper-layer zonal wind maximum is located inside the Ferrel cell with strong westerlies below, while for $H \geq 9.7$ in set H and $r \geq 1.2$ in set r the latitude of the maximum zonal wind shifts abruptly toward the Hadley cell edge with zero surface winds below. At the same point in the parameter space, marked by vertical solid lines in Fig. 2, the meridional circulation and the surface winds become much weaker. This is clearly a transition between two flow regimes: the latter (with $H \geq 9.7$ and $r \geq 1.2$) has the characteristics of a subtropical jet regime, while the former (with $H \leq 9.6$ and $r \leq 1$) can be viewed either as an eddy-driven or a merged jet regime. A closer look reveals that for $H \leq 8.5$ and $r \leq 0.5$, the system is in a double jet regime, with a weak subtropical jet and a strong eddy-driven jet, and for $8.8 \leq H \leq 9.6$ and $0.7 \leq r \leq 1$ the two jets merge into one, so we refer to it as a merged jet regime. The transition from a double jet to a merged jet regime is marked

by vertical dashed lines in Fig. 2. The difference between the double and merged jet regimes is manifested not only by the existence of a weak subtropical jet inside the Hadley cell but also by a change in the dominant wavenumbers (Fig. 4, described below), a change in the local Rossby number near the Hadley cell edge (Figs. 2e,f, described below), and a change in the time variability of the zonal mean zonal wind (not shown), which is characterized by meandering of the jet in the double jet regime and pulsing of the jet in the merged jet regime. The double jet regime and the transition between it and a merged jet regime have been dealt with in the literature (Son and Lee 2005; Gerber and Vallis 2007; Eichelberger and Hartmann 2007) and we will refer to them in a subsequent paper. Here we shall focus on the more abrupt transition between the merged jet regime and the subtropical jet regime, which has not received much attention.

As explained in the introduction, we expect to find that a subtropical jet would be driven mainly by advection of planetary momentum by the MMC inside the Hadley cell. According to Eq. (1), in a steady state with a meridional circulation and no wave fluxes, the advection of planetary momentum by the MMC, represented by the Coriolis force, is balanced by the advection of relative momentum by the MMC and the absolute angular momentum is conserved (Held and Hou 1980). In this state, the local Rossby number, which is defined as minus the vorticity of the zonal mean flow divided by the Coriolis parameter [Ro $= -\overline{\zeta_1}/f$, where $\overline{\zeta_1} = -[\partial \cos(\phi)\overline{u_1}]/[a\cos(\phi)\partial\phi]$ and $f = 2\Omega\sin(\phi)$], would be equal to 1 (Walker and Schneider 2006; Schneider and Bordoni 2008). As the Rossby number is closer to zero, the negative EMFC inside the Hadley cell is stronger, meaning that the eddies weaken the zonal mean wind inside the Hadley cell. Figures 2e and 2f show the Rossby number as a function of parameter and latitude, with lines marking the subtropical Hadley cell edge. Since the Rossby number is not well defined near the equator, we show its values only at latitudes higher than 10°S. In the merged jet regime, the Rossby number does not exceed 0.3 in the latitudes between 15°S and the edge of the Hadley cell, which means that the main balance there is between the EMFC and the Coriolis force. At the transition between the double jet and merged jet regimes,
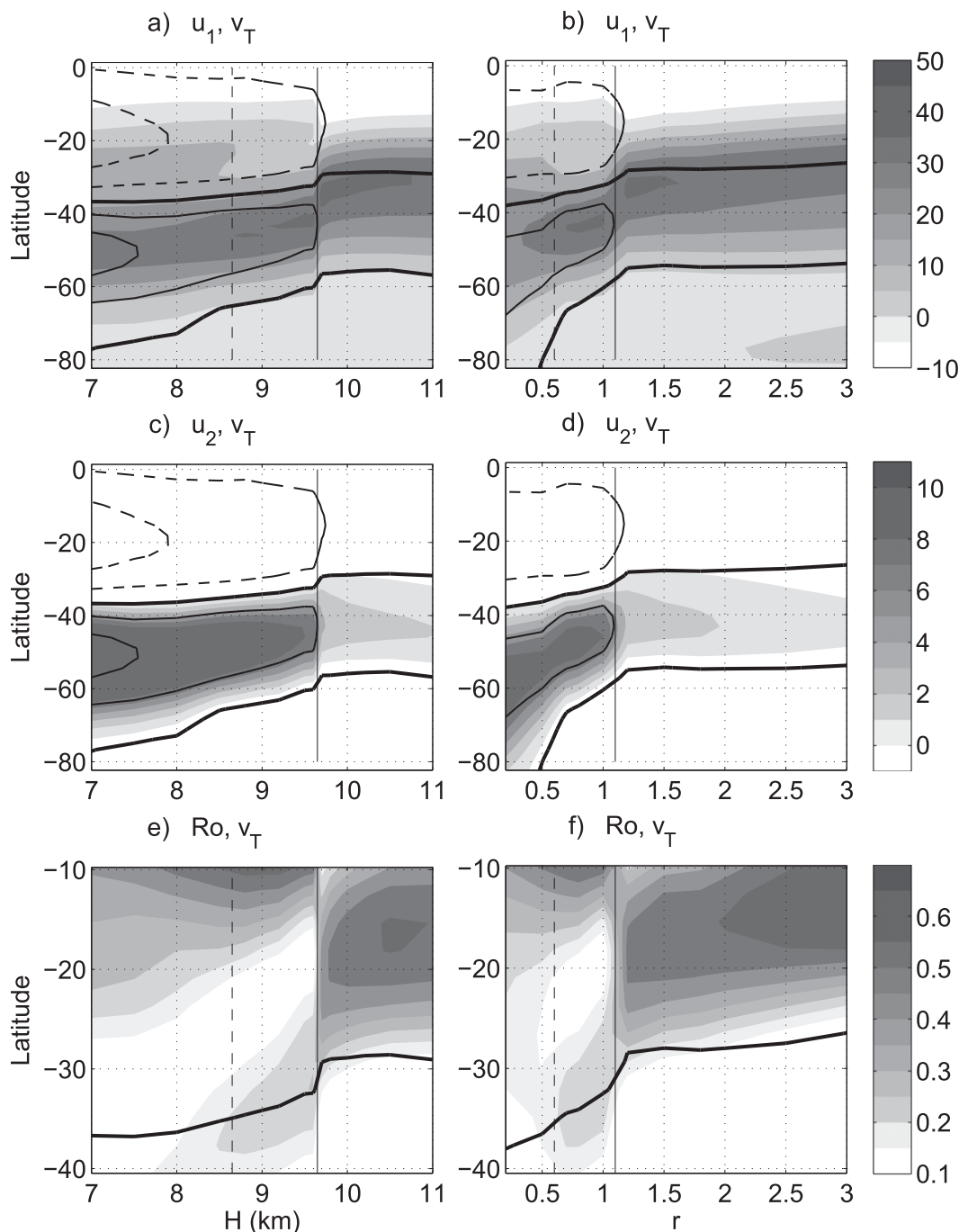
FIG. 2. Mean-flow time-averaged variables for the parameter sweeps from set H and set r (see Table 1) as a function of latitude and parameter. Zonal wind in the (a),(b) upper layer and (c),(d) lower layer (shading, $m\,s^{-1}$). Baroclinic meridional wind (contour interval is $0.2\,m\,s^{-1}$). Thin dashed and thin solid contours represent negative and positive values, respectively. Thick contour is for $v_T = 0$, marking the edges of the circulation cells. (e),(f) Local Rossby number (Ro, shading; see text). Thick contour is for $v_T = 0$. (left) Set H and (right) set r. Vertical dashed and solid lines mark the transitions from a double jet to a merged jet regime and from a merged jet to a subtropical jet regime, respectively (see text).

there is a slight increase in the Rossby number near the Hadley cell edge, meaning that the degree of angular momentum conservation at the subtropics in the merged jet regime is higher than in the double jet regime, which gives further justification to classify this regime as merged rather than eddy driven. At the transition to the subtropical jet regime, the Rossby number becomes higher than 0.6 inside the Hadley cell. This means that indeed in the subtropical jet regime the advection of relative momentum by the MMC becomes larger than the EMFC, although the EMFC is still significant since the Rossby number is less than 1.

To further investigate the transition, we look at the wave fluxes for set H. Set r and set D show qualitatively similar results. Figure 3a shows the EMFC in the upper layer and the southward eddy heat flux as a function of latitude and H. The EMFC is defined as $\text{EMFC}_1 = -(1/a\cos^2\phi)\{\partial[\cos^2\phi\overline{(u_1'v_1')}]/\partial\phi\}$ and the southward heat flux is $(-\overline{V'b'})$, where b' is the wave's buoyancy [see Eq. (A2)]. It is seen that both the EMFC and the heat flux become weaker at the transition to the subtropical jet regime. The eddy kinetic energy (not shown) also shows an abrupt decrease at the transition. In the merged jet regime, the heat flux is maximal close to the jet latitude where $\overline{u_1}$ is maximal, while in the subtropical jet regime, it is displaced to higher latitudes far from the jet. For example, for $H = 9$ km, $\overline{u_1}$ is maximal around 45°S and the heat flux is maximal around 40°S, while for $H = 11$ km, $\overline{u_1}$ is maximal around 30°S and the heat flux is maximal around 50°S.

An explanation of the jet-type transition should include the mutual interactions between the waves and the mean flow. In terms of the effect of waves on the mean flow, the above results show that a merged jet is maintained when eddy kinetic energy and fluxes are stronger and a subtropical jet exists when eddies are weaker and less able to displace the jet poleward. In addition, both the EMFC and the heat flux in the subtropical jet regime are not only weaker, but also located far poleward of the jet core, allowing for a subtropical jet to be maintained by a balance mainly between the Coriolis force and the advection of momentum by the MMC, expressed by a large Rossby number. In terms of the effect of the mean flow on the waves, an explanation is needed for the abrupt decrease in wave energy at the transition to the subtropical jet regime, noting that the subtropical jet has a stronger vertical shear, and so it may be expected to be a source for stronger baroclinic instability. The change in the heat flux latitudinal structure suggests that in the subtropical jet regime, baroclinic instability occurs at latitudes much higher than the jet latitude. To better understand the effect of the mean flow on the waves, we look at the mean PV gradient.
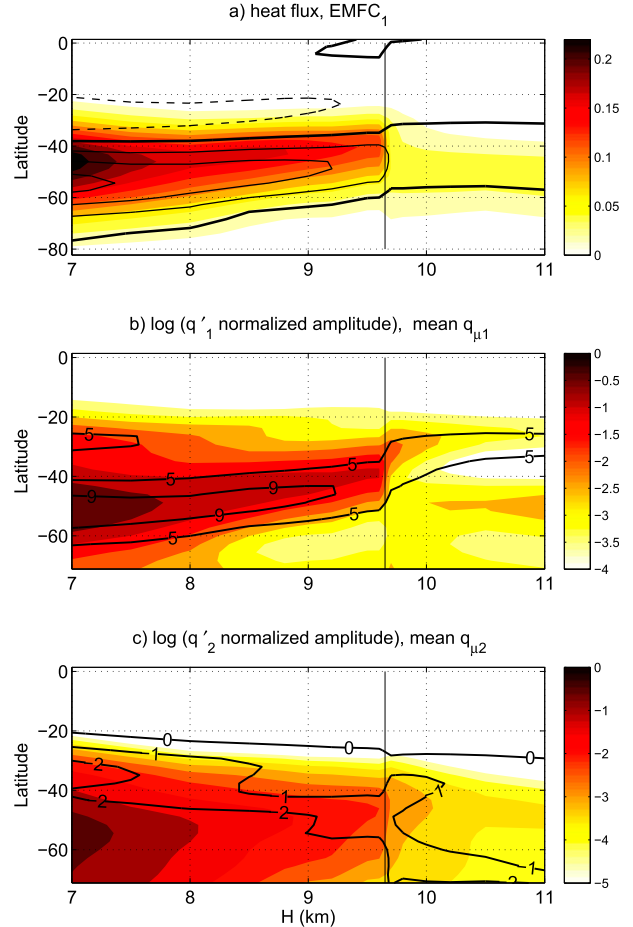

FIG. 3. Zonal and time averages of the wave fluxes and amplitudes and the PV gradients for set H (see Table 1) as a function of latitude and H (km). (a) Southward eddy heat flux, defined as $(-\overline{V'b'})$ [see Eq. (A2)] (shading, $\text{m}^2\,\text{s}^{-3}$) and upper-layer eddy momentum flux convergence (contour interval $2 \times 10^{-5}\,\text{m}\,\text{s}^{-2}$). Thin dashed, thin solid, and thick solid contours represent negative, positive, and zero values, respectively. (b) Shading represents the logarithm of the normalized upper-layer wave PV amplitude (see text). Contours represent the mean upper-layer PV gradient, with contour values 5×10^{-4} and $9 \times 10^{-4}\,\text{s}^{-1}$. (c) As in (b), but for the lower layer with contour values 0, -1×10^{-4}, and $-2 \times 10^{-4}\,\text{s}^{-1}$. Vertical solid line marks the transition from a merged jet to a subtropical jet regime (see text).

Figures 3b and 3c show the mean PV gradient and the logarithm of the normalized wave PV amplitude for both layers for set H. The other two sets show a qualitatively similar behavior. The wave PV amplitude is defined as the time average of $[\overline{(q')^2}]^{1/2}$. The logarithm was taken to allow easy comparison between model integrations since the wave PV amplitude assumes a wide range of values. Normalization is done by the maximum over H and latitude. In the merged jet regime, the upper-layer wave amplitude is maximal where the upper-

PV gradient is maximal, which is at the jet core (around 45°S for $H = 9$ km), and the lower-layer wave amplitude is maximal at the same latitudes, but with a much wider distribution. In the subtropical jet regime. the upper-layer wave amplitude has two local maxima: one where the upper-layer PV gradient is maximal, near the jet core (around 25°S for $H = 11$ km), and the other above the lower-layer maximum wave amplitude (around 50°S for $H = 11$ km). The lower-layer PV gradient is positive at the latitude of the jet and equatorward of it in the subtropical jet regime, as seen by the area above the zero contour in Fig. 3c. Since the Charney and Stern criterion for baroclinic instability (Charney and Stern 1962) requires that the PV gradient would change sign inside the domain and since the upper-layer PV gradient is positive everywhere, this configuration of the PV gradient causes the lower-layer wave PV amplitude and the eddy heat flux to be concentrated where the lower-layer PV gradient is negative, far poleward of the jet core in the subtropical jet regime. It should be noted that the reason for the positive PV gradient at low latitudes is the β effect: the meridional gradient of the planetary vorticity. The contribution of β to the PV gradient is not affected by the mean flow, but as the jet moves equatorward, it becomes closer to the latitude where β is large enough to make the lower-layer PV gradient positive.

The above results suggest that the mechanism of the jet-type transition is as follows. At upper levels, the large PV gradients associated with the meridional curvature of the jet act to concentrate the upper-level waves at the jet core. As the jet moves equatorward closer to the latitude at which the β effect dominates and makes the lower-level PV gradient positive, as in the subtropical jet regime, baroclinic instability becomes less efficient. The baroclinically unstable normal modes, which grow because of a mutual amplification and phase locking of the upper-level waves on the positive PV gradient region, and the lower-level waves on the negative PV gradient region are now tilted equatorward with height, which makes their interaction less efficient (Heifetz et al. 2004). This reduction in the efficiency of the instability causes the waves to saturate at a lower amplitude so that their poleward momentum flux becomes weaker and the jet is shifted equatorward to the edge of the Hadley cell, where it is maintained by the advection by the MMC, thus creating a positive feedback loop. This feedback may explain the abruptness of the transition. The fact that set r shows the same regime transition as in set H indicates that it is the change in the amplitude of the waves that triggers the regime transition as H is varied.

A decrease in the wave energy as the subtropical jet becomes stronger was found also in the observational studies of Nakamura and Sampe (2002) and Nakamura

and Shimpo (2004), which showed that when the subtropical jet is strong, the upper-level waves are trapped in the jet core and are separated from the lower-level baroclinic zone in the midlatitudes, making the baroclinic interaction inefficient. It should be noted that the confinement of the lower-level waves to middle and high latitudes was attributed in these studies to the location of the oceanic frontal zone that maintains the low-level baroclinicity and not to the β effect as we find in our model. They use the Eady growth rate as a measure of baroclinicity, as commonly used, yet this measure ignores the β effect, which also affects the baroclinicity.

4. Spectral analysis of the waves

a. Waves in the model

The structure and intensity of the wave heat and momentum fluxes change significantly at the transition from a merged to a subtropical jet regime, as seen in Fig. 3. It is useful to look at the spectral properties of the waves in order to understand better the source of this change in the wave structure and how it is controlled by the shape of the mean flow in each regime. Figure 4 shows the logarithm of the power spectrum of the upper-layer wave PV, normalized by its maximum value ($\log\{P(q_1')/\max[P(q_1')]\}$, where P is the power spectrum), as a function of the zonal wavenumber m and H for set H. The normalization is done in order to compare easily between integrations with different parameters and different wave amplitudes. The transition in the type of jet is accompanied by a transition in the dominant wavenumbers: in the merged jet regime ($8.8 \leq H \leq 9.6$) wavenumber 5 is the most dominant, while in the subtropical jet regime ($H \geq 9.7$), it is significantly weaker, and wavenumbers 2 and 3, which become slightly stronger, are the dominant ones. The transition from a double jet to a merged jet regime described in section 3 is clearer when looking at the spectrum, which changes from being relatively wide and dominated by wavenumber 4 in the double jet regime ($H \leq 8.5$) to the narrow spectrum of the merged jet regime with a dominant wavenumber 5.

Figure 5 shows the upper-layer EMFC phase speed spectra and the time-averaged $\overline{u_1}$ and $\overline{u_2}$ for two examples from set H: the $H = 9$ km integration, denoted by "MJ" (Fig. 5a), which is an example of a merged jet regime integration, and the $H = 10$ km integration, denoted by "STJ" (Fig. 5c), which is an example of a subtropical jet regime integration. Other integrations from each regime show qualitatively similar results. The EMFC spectra were calculated according to the method described in Randel and Held (1991) as the phase speed cospectra
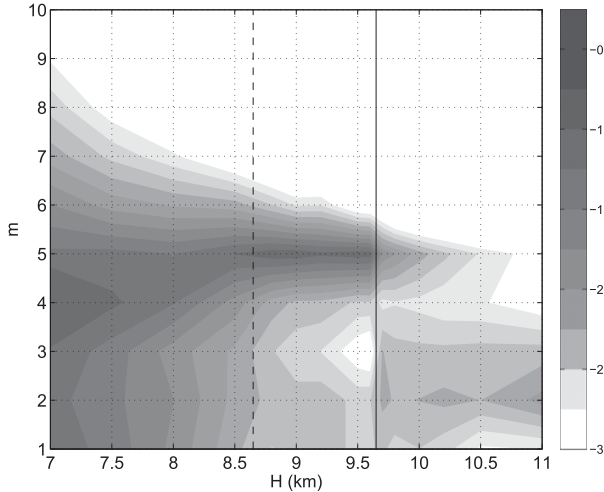
FIG. 4. Logarithm of the averaged normalized upper-layer wave PV power spectrum, $\log\{P(q_1')/\max[P(q_1')]\}$, as a function of m and H (km) for set H. Averaging is over time and latitude in the Southern Hemisphere. Vertical dashed and solid lines mark the transitions from a double jet to a merged jet regime and from a merged jet to a subtropical jet regime, respectively (see text).

of v_1' and ζ_1'. Lines of constant angular phase speed were added for reference. For each line, the phase speed is $c = c_0\cos(\phi)$, where in Fig. 5a $c_0 = 18$ and $26\,\mathrm{m\,s^{-1}}$ and in Fig. 5c $c_0 = -4$ and $9\,\mathrm{m\,s^{-1}}$. Figures 5b and 5d show the time and zonal average of the total EMFC as a function of latitude for the two integrations.

For the merged jet example ($H = 9\,\mathrm{km}$; Fig. 5a), the strong convergence of eddy momentum flux at the midlatitudes and divergence at the subtropics are contributions from waves with relatively well defined phase speeds. The lines of constant angular phase speed with $c_0 = 18$ and $26\,\mathrm{m\,s^{-1}}$ fit well with the two major peaks of the EMFC. Slower and faster waves have weaker contributions. A decomposition of the EMFC phase speed spectrum to contributions from different wavenumbers (not shown) shows that the convergence at midlatitudes around the $c_0 = 26\,\mathrm{m\,s^{-1}}$ line comes from wavenumbers 4–6, while the divergence at the subtropics comes from wavenumbers 5 and 6. The convergence and divergence around the $c_0 = 18\,\mathrm{m\,s^{-1}}$ line comes mainly from wavenumber 5. The divergence near 70°S at very low phase speed comes from wavenumber 2.

For the subtropical jet example ($H = 10\,\mathrm{km}$; Fig. 5c), there is very little divergence of eddy momentum flux at the subtropics and the EMFC pattern shows mainly convergence at the midlatitudes and divergence at high latitudes, which come from a relatively wide range of phase speeds. The peak of the convergence at midlatitudes (around 45°S) is around the line of $c_0 = 9\,\mathrm{m\,s^{-1}}$, with

a secondary peak at a lower phase speed near latitude 35°S. The divergence at high latitudes has two major peaks near the lines $c_0 = -4$ and $9\,\mathrm{m\,s^{-1}}$, with contributions also from phase speeds in between and lower. A decomposition of the EMFC phase speed spectrum to contributions from different wavenumbers (not shown) shows that the convergence at midlatitudes around the $c_0 = 9\,\mathrm{m\,s^{-1}}$ line comes from wavenumbers 3 and 4, while the secondary peak at the subtropics comes from wavenumber 5. The high-latitude divergence around the $c_0 = 9\,\mathrm{m\,s^{-1}}$ line comes from wavenumbers 3–5, while the divergence from the westward-propagating waves ($c_0 = -4\,\mathrm{m\,s^{-1}}$ and lower) comes from wavenumbers 1–3 and 5.

The picture that arises from this analysis is that there is a range of modes that may be divided into two main categories: westward-propagating slow long waves (wavenumbers 1–3), which contribute to eddy momentum flux divergence at high latitudes, and eastward-propagating intermediate scale waves (wavenumbers 4–6) at midlatitudes, which contribute to eddy momentum flux convergence at the midlatitudes and divergence at the subtropics and high latitudes. Both types of modes exist in both regimes, while the intermediate-scale midlatitude modes are more dominant in the merged jet regime and the long high-latitude modes are more dominant in the subtropical jet regime. In addition, the phase speed of the intermediate-scale midlatitude modes is slower in the subtropical jet regime, which may be attributed to the weaker surface westerlies. The Fjørtoft criterion for instability (Fjørtoft 1950) requires that $\bar{u} - c$ have the same sign as the PV gradient, which means that the phase speed should exceed the lower-layer mean wind speed. As seen in Fig. 5 in both cases, the phase speed is always above, or very close to, the lower-layer zonal mean wind speed.

An analysis of the normal modes of the time-averaged mean flow for each case may add another insight to the effect of the mean flow on the dominant modes. Figure 6 shows properties of the three leading normal modes for each of the examples shown in Fig. 5. The normal modes are the eigenvectors of the linear wave equations when the mean flow is the time-averaged $\overline{u_1}$ and $\overline{u_2}$ in the upper and lower layers, respectively. The linear equations are Eqs. (A10a) and (A10b) but without the nonlinear wave–wave terms and without the radiative damping, friction, and numerical diffusion terms. The leading modes are the modes with the highest growth rate from all zonal wavenumbers. Figures 6a and 6c show the upper-layer wave PV amplitude for each normal mode $|q_1|$ and the upper-layer time-averaged wave PV amplitude from the model (defined in section 3) as a function of latitude, each normalized by its maximum value.
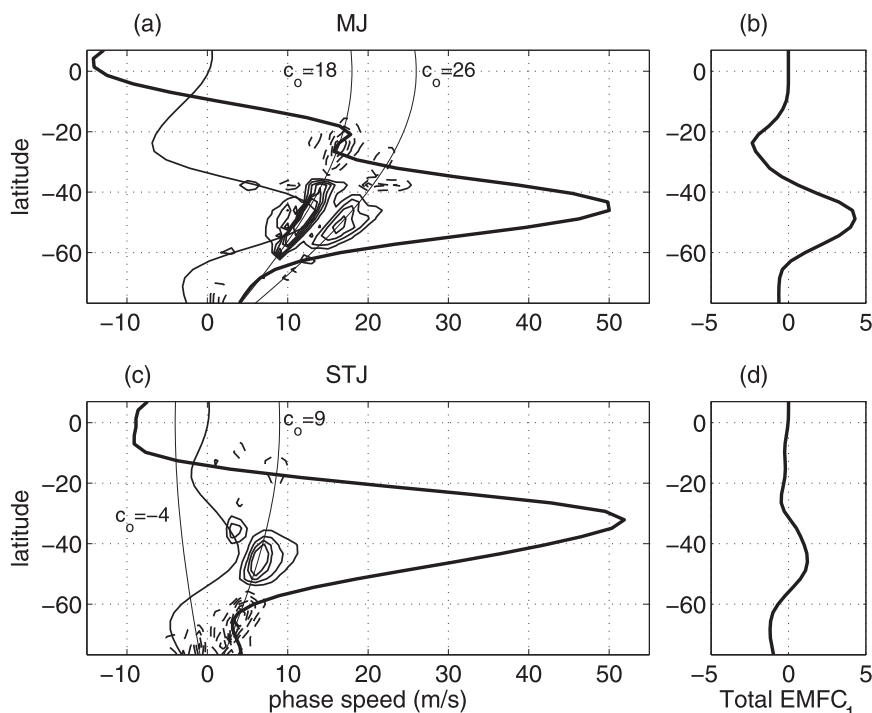
FIG. 5. $EMFC_1$ for two integrations: "MJ" and "STJ" (see text). (a),(c) Phase speed co-spectra of $EMFC_1$ (contours), $\overline{u_1}$ (thick line), and $\overline{u_2}$ (intermediate line), and lines of constant angular phase speed (thin lines with annotations showing the values of c_0; see text). Solid and dashed contours represent positive and negative values, respectively. Contour interval for the cospectrum is $10^{-6}\,\mathrm{m\,s^{-2}}$ in (a) and $0.5 \times 10^{-6}\,\mathrm{m\,s^{-2}}$ in (c). (b),(d) Time-mean and zonal mean $EMFC_1$ for the same two integrations ($10^{-5}\,\mathrm{m\,s^{-2}}$).

For both examples, there is a clear connection between the latitudinal structure of the waves in the model and that of the leading normal modes. For the merged jet example, there is a peak in the amplitude near the jet maximum (Fig. 6a, thick vertical dashed line), both in the model and for the three leading normal modes (that have wavenumbers 5, 6, and 4). A secondary peak around 75°S comes from longer waves, which correspond to normal modes with a weaker growth rate (not shown). For the subtropical jet example there are two peaks that are similar to those of the normal mode with wavenumber 4: one around 30°S near the jet core (Fig. 6c, thick vertical dashed line) and the other around 50°S, near the maximum amplitude of the lower-layer wave (see Fig. 3c, at $H = 10$). Another peak around 75°S fits well with the peak of the normal modes with wavenumbers 2 and 3. In both examples, the intermediate-scale normal modes have sharp peaks at the critical levels, which do not appear in the model owing to nonlinear wave breaking and numerical diffusion. The critical levels are marked by thin vertical dashed lines in Figs. 6a and 6c and are calculated by taking $c_0 = 26$ and $c_0 = 10\,\mathrm{m\,s^{-1}}$ in the MJ and STJ examples, respectively.

The connection between the modes in the model and the linear normal modes is further established by comparing their phase speeds. The three leading normal modes in the merged jet example are obtained for wavenumbers 5, 6, and 4 and have phase speeds $c_0 = 25.4$, 26.5, and $25.1\,\mathrm{m\,s^{-1}}$, respectively, which fits well with the line of $c_0 = 26\,\mathrm{m\,s^{-1}}$ in Fig. 5a. The line of $c_0 = 18\,\mathrm{m\,s^{-1}}$ in Fig. 5a is related to another mode, which is the second most unstable mode for wavenumber 5. The three leading normal modes in the subtropical jet example are obtained for wavenumbers 2–4 and have phase speeds $c_0 = -7.7$, -4.3, and $10.1\,\mathrm{m\,s^{-1}}$ respectively. The westward-propagating long normal modes are related to the modes in the model near the $c_0 = -4\,\mathrm{m\,s^{-1}}$ line in Fig. 5c, while the third normal mode (with wavenumber 4) is related to the modes near the line $c_0 = 9\,\mathrm{m\,s^{-1}}$.

Figures 6b and 6d show the latitudinal structure of the EMFC for the three leading normal modes and for the model. The convergence of eddy momentum flux in the merged jet example near 50°S seen in Figs. 5a and 5b appears also for the leading normal modes. The divergence at the subtropics and high latitudes is more spread over latitude in the model than for the linear modes, as
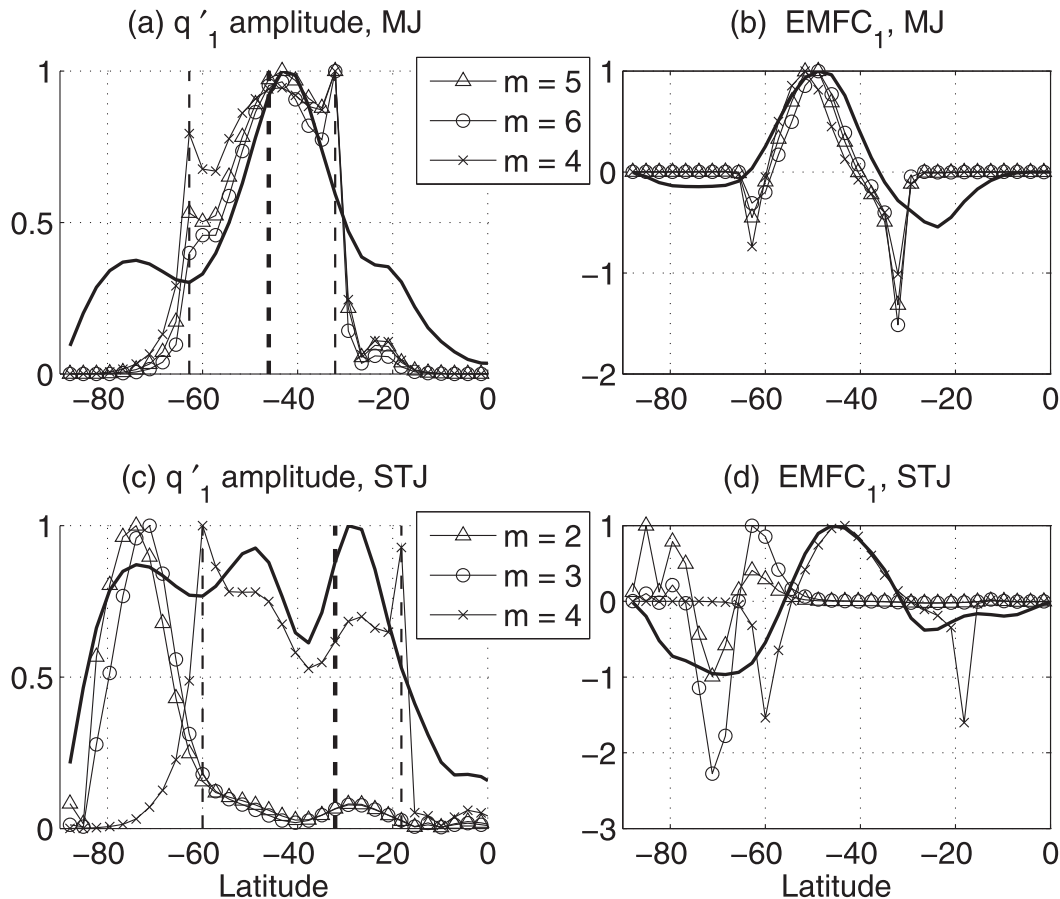
FIG. 6. (a),(c) Normalized upper-layer wave PV amplitudes (as defined in the text) and (b),(d) EMFC from the model (thick lines) and for the three leading normal modes (marked lines) for the same two integrations as in Fig. 5. Thick and thin vertical dashed lines mark the locations of the jet core and critical levels, respectively, where the critical levels for the MJ and STJ examples are for $c_0 = 26$ and $10 \, \mathrm{m \, s^{-1}}$, respectively. All variables are normalized by their maximum values. Legends show the zonal wavenumber of the respective normal mode, ordered according to the growth rate (fastest growing mode first).

may be expected owing to nonlinear wave breaking. In the subtropical jet example, the convergence at the midlatitudes fits well with the EMFC pattern of the mode with wavenumber 4, while the strong divergence at high latitudes is collocated with that of the first two modes that have wavenumbers 2 and 3.

The above analysis shows that the configuration of the mean flow in each regime "selects" the dominant modes by allowing specific normal modes to grow faster. In the merged jet regime, when the jet is located at the midlatitudes and the surface winds are strong, the modes that grow most efficiently are intermediate-scale modes with relatively high phase speeds. In the subtropical jet regime, when the upper-layer jet is located at lower latitudes where the β effect suppresses baroclinic instability, the growth of the intermediate-scale waves at midlatitudes is weaker and their phase speeds are lower

because of the weaker surface westerlies. Long westward-propagating waves become dominant, growing baroclinically at high latitudes where the surface wind is westward and the upper-layer wind is eastward. These waves are trapped at high latitudes, since the surface winds are eastward at the midlatitudes, violating the Fjørtoft criterion for instability.

b. Comparison with Southern Hemisphere observations

The properties of the wave fluxes found in each regime in the model can be compared with those of similar regimes in the atmosphere. The merged jet and subtropical jet regimes in the model may be compared with the Southern Hemisphere summer and winter climatology, respectively (see Fig. 1). We prefer not to relate to the Northern Hemisphere winter, since it is characterized

by a strong breaking of the zonal symmetry,[1] which does not exist in the model, and not to the Northern Hemisphere summer, when the jet is weak and more difficult to classify.

Figure 7 shows plots of the spectra of the wave fluxes in the Southern Hemisphere winter and summer, taken from the observational studies of Randel and Held (1991) and Kim and Lee (2004). Figures 7a–d show the EMFC at 300 hPa and heat flux at 700 hPa from transient eddies as a function of latitude and phase speed for the Southern Hemisphere winter and summer, from Kim and Lee (2004). Figures 7e and 7f show the heat flux as a function of wavenumber and phase speed for 47°S in summer and winter, from Randel and Held (1991). In the Southern Hemisphere summer, the heat flux and EMFC are both maximal around the jet latitude (between 45° and 55°S) and the peak of their spectrum is at relatively high wavenumbers (wavenumber 6) and large phase speeds (10–15 m s^{-1}), while in the Southern Hemisphere winter the heat flux maximum (at 45°–65°S) is far from the jet latitude (at 25°–30°S), and its spectrum is maximal at lower wavenumbers (4 and 5) and lower phase speeds (5–10 m s^{-1}) and the EMFC is slightly weaker and comes mainly from slow waves (5–10 m s^{-1}) at latitudes around 35°S and fast waves (10–15 m s^{-1}) at midlatitudes (around 50°S). At high latitudes (60°–80°S), there is an increase in the heat flux and eddy momentum flux divergence at very low and negative (westward) phase speeds in winter compared to summer. These fluxes at high latitudes can be attributed to long waves (wavenumbers 1–3; e.g., Mechoso and Hartmann 1982).

These characteristics of the heat flux and EMFC in the Southern Hemisphere summer and winter are very similar to what we find in our model's merged and subtropical jet regimes, respectively (Figs. 3a, 4, and 5), only in our model the fast waves in the subtropical jet regime are very weak and accordingly the total EMFC at the midlatitudes is weak unlike in the Southern Hemisphere

winter, probably due to the fact that while the flow regime in the Southern Hemisphere winter is a double jet regime in which the subtropical jet is stronger than the eddy-driven jet, the subtropical jet regime in our model does not have a significant eddy-driven jet. The resemblance of the properties of the waves in our model to those of the waves in the appropriate regimes in the atmosphere implies that the mechanism of the transition found in the model may be relevant for the atmosphere as well.

5. The effect of tropical heating

As shown in section 3 for the parameter sweeps of sets H and r, a transition from a merged jet regime to a subtropical jet regime occurs when the MMC and the wave fluxes both become weaker. The parameters H and r both control the wave energy and the transition implies that a feedback between the waves and the mean flow is present. To assess the relevance of the results to the atmospheric flow and to compare with previous studies, we examine the effect of a change in the external forcing on the regime transition. For this purpose, we performed a parameter sweep over the parameter D (set D in Table 1), which multiplies a term of tropical diabatic heating in the heat equation (see section Ac). The values of the parameters H and r, which were held constant is set D, were chosen so that for $D = 0$, the system is in the subtropical jet regime. Figure 8 shows $\overline{u_1}$ and $\overline{v_T}$ (Fig. 8a) and $\overline{u_2}$ and $\overline{v_T}$ (Fig. 8b) as a function of latitude and D. Figure 8c shows the Rossby number as a function of latitude and D, with lines marking the subtropical Hadley cell edge.

It is seen from Fig. 8 that for low tropical heating ($D \leq 0.5$), the flow is in the subtropical jet regime and for high tropical heating ($D \geq 0.65$), there is a transition to the merged jet regime, similar to the transitions seen in Fig. 2 when H and r are decreased. The transition to a merged jet regime as the tropical heating is increased is due to the enhancement of the MMC: as the tropical heating is increased, the Hadley circulation becomes stronger, since the adiabatic cooling associated with the rising branch of the Hadley cell acts to balance the diabatic heating. As the mean meridional wind becomes stronger, the EMFC becomes stronger as well, which is consistent with the momentum balance condition for the zonal mean flow expressed in Eq. (1), leading to a transition to a merged jet regime.

The transition to a merged jet regime as the Hadley cell strengthens may seem unrealistic, since in the atmosphere a subtropical jet is observed mainly in winter when the Hadley cell is strong. However, a comparison with other numerical and observational studies offers a few possibilities for interpreting this connection between tropical heating and the dominant type of jet.

---

[1] In the Northern Hemisphere winter, different flow regimes may be identified by zonally averaging over certain longitudinal sectors (Eichelberger and Hartmann 2007). A classification of these regimes according to the categorization suggested in this paper will be discussed in a separate paper, but it should be mentioned that when looking at the location of the maximum zonal wind relative to the latitudes of ascent and decent, it seems that above the Pacific Ocean the jet is located inside the Ferrel cell, similar to the merged jet regime, while above Asia, it is closer to the edge of the Hadley cell, similar to the subtropical jet regime. However, comparing the dominant modes raises the possibility that the regime above the North Pacific is close to the subtropical jet regime, since westward-propagating long waves in high latitudes were observed there by Kushnir (1987), similar to what we find in the subtropical jet regime in our model.
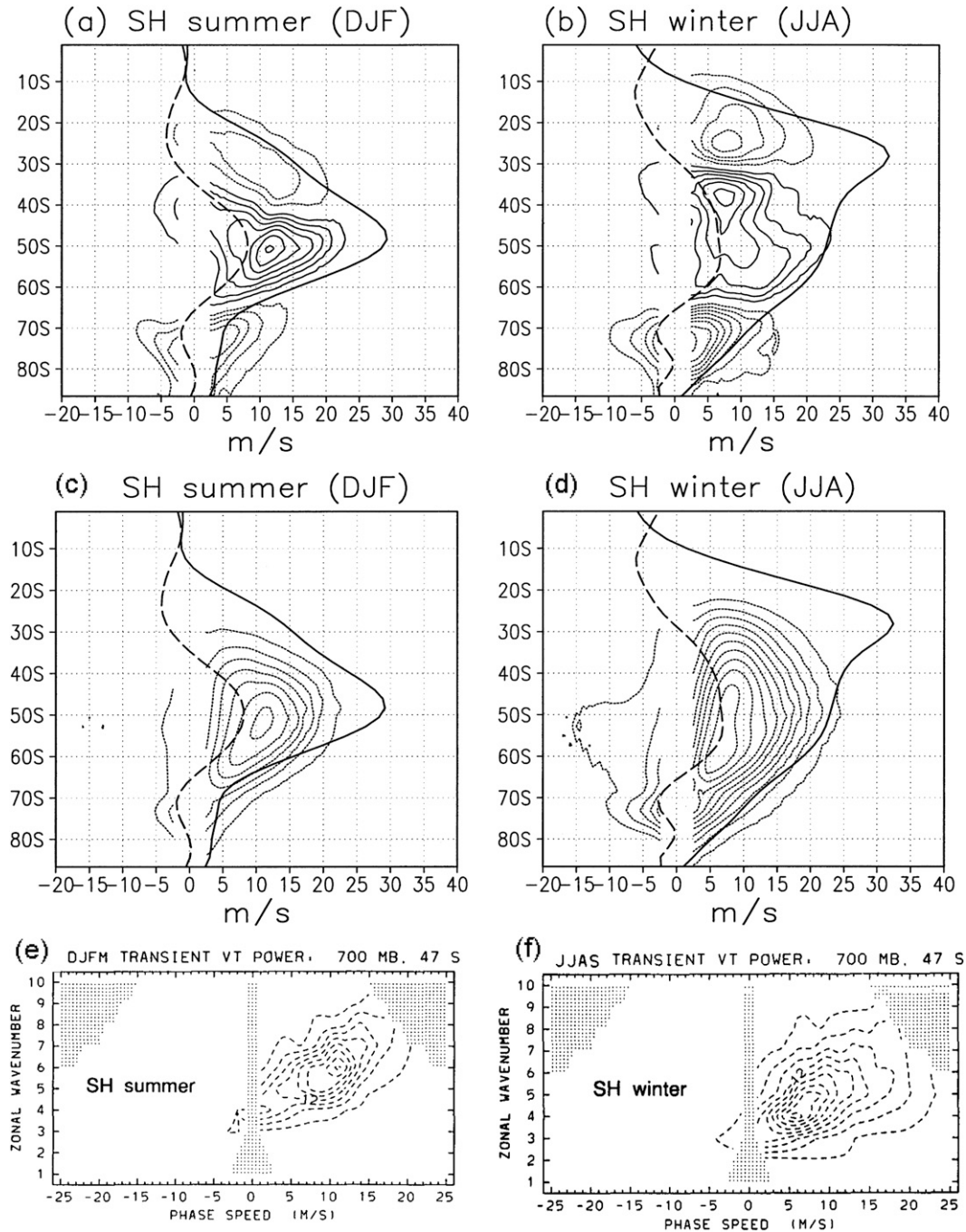
FIG. 7. (a),(b) Cospectra of the EMFC at 300 hPa as a function of zonal phase speed and latitude for the SH summer and winter. Contour interval is $2 \times 10^{-7} \, \mathrm{m \, s^{-2}}$ and zero contours are omitted. Solid (dotted) contour lines represent the eddy momentum flux convergence (divergence). Thick solid and dashed lines represent the 300 hPa and the surface zonal mean zonal winds, respectively. (c),(d) Eddy meridional heat flux at 700 hPa for the SH summer and winter. Contour interval is $0.05 \, \mathrm{K \, m \, s^{-1}}$ and zero contours are omitted. Solid (dotted) contour lines represent the equatorward (poleward) eddy meridional heat flux. (e),(f) Wavenumber–phase speed covariance spectra for mid-latitude (47°) low-level (700 hPa) heat flux for the SH summer and winter. Contour interval is $0.03 \, \mathrm{K \, m \, s^{-1}} \, \Delta c^{-1}$. (a)–(d) After Kim and Lee (2004) and (e),(f) after Randel and Held (1991).
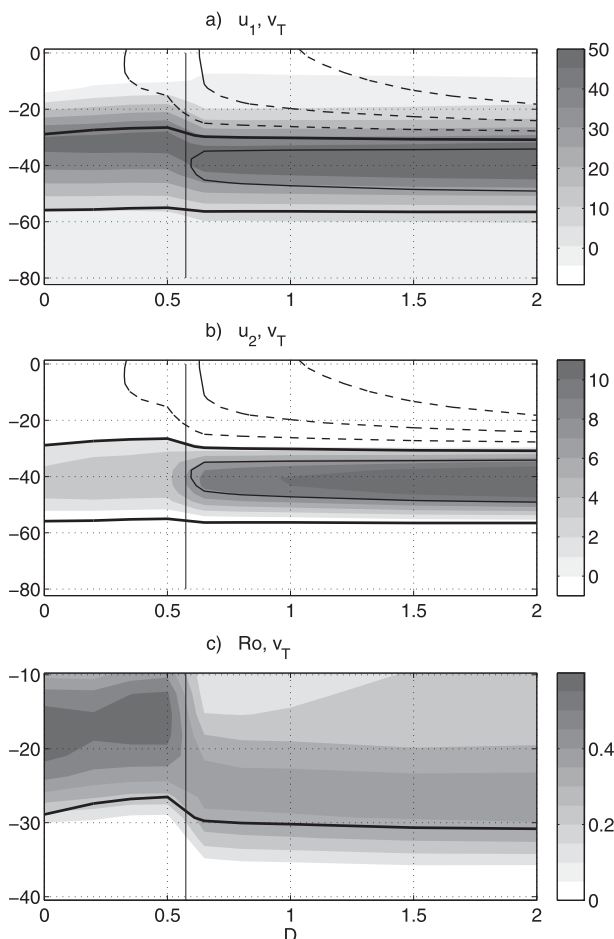
FIG. 8. As in Fig. 2, but for set D. Vertical solid line marks the transition from a subtropical jet to a merged jet regime (see text).

The results of set D should be compared with cases in which tropical heating was increased when the reference state had a single subtropical jet at the edge of the Hadley cell. Many studies examined the effect of increased tropical heating when the reference state had either a double jet or a single jet inside the Ferrel cell (Chang 1995; Son and Lee 2005; Eichelberger and Hartmann 2007; Lu et al. 2010). The only study that we have found in which the jet in the reference state is subtropical is that of Robinson (2006), who found a transition from a subtropical jet regime to a self-maintaining jet regime as the pole-to-equator temperature difference is increased, which is equivalent to increasing the tropical heating. Although his self-maintaining jet regime is similar to our merged jet regime, the subtropical jet in Robinson (2006) is unrealistically weak.

A subtropical jet can be maintained in a limited longitudinal sector when an enhanced Hadley circulation with a zonally asymmetric pattern is added to a reference state with a single jet inside the Ferrel cell, as shown by Brayshaw et al. (2008). They add a zonally asymmetric sea surface temperature anomaly at the subtropics, which has an effect on the Hadley circulation equivalent to an anomaly in the diabatic heating at the tropics. As seen in their Fig. 8, a single subtropical jet exists downstream of the enhanced Hadley circulation, and a single eddy-driven jet exists downstream of the weakened Hadley circulation, with a double jet farther downstream. The subtropical jet in this case is stronger than the eddy-driven jet, as in the Southern Hemisphere winter. The results of Brayshaw et al. (2008) suggest that the strong zonal asymmetry in winter in the real atmosphere contributes to the dominance of the subtropical jet.

The longitudinal profile of the upper-tropospheric zonal wind and synoptic-eddy (time scale of 9 days and less) poleward heat flux is shown in Fig. 9 for the Southern Hemisphere winter [June–August (JJA)] and summer [December–February (DJF)]. In the Southern Hemisphere summer, the jet is merged and collocated with the heat flux at all longitudes. In the Southern Hemisphere winter, the subtropical jet is dominant in a limited longitudinal sector (over the eastern Indian Ocean, Australia, and the western and central Pacific), while the heat flux is strongest at different longitudes (poleward of Africa and over the western and central Indian Ocean). This means that the coexistence of a strong subtropical jet and strong eddy activity seen in the zonal mean climatology of the Southern Hemisphere winter is an artifact of the zonal averaging and cannot be explained by a balanced state existing in a statistically zonally symmetric model. The observational study of Williams et al. (2007) supports this possibility, showing that the spiral form of the Southern Hemisphere jet during autumn is maintained by synoptic eddies that transfer momentum poleward from the subtropical jet to the eddy-driven jet farther downstream. Williams et al. (2007) showed also a few numerical integrations in which they added a localized tropical heating to a statistically zonally symmetric model. These integrations reproduced the spiral form of the jet for a limited time, after which a state dominated by a merged jet prevailed, suggesting that the spiral jet represents a transient phase and not a statistically steady state.

To conclude, in a statistically zonally symmetric situation with a dominant subtropical jet, increasing the tropical heating may lead to a transition to a merged jet regime. However, when tropical heating is enhanced in a zonally localized sector it intensifies the subtropical jet locally and increases the wave energy farther downstream, enabling the subtropical jet to be maintained in a limited sector. This situation seen in autumn and winter may be a manifestation of a transient phase and not a statistically steady state. It is also possible that the dominance of the subtropical jet in winter compared
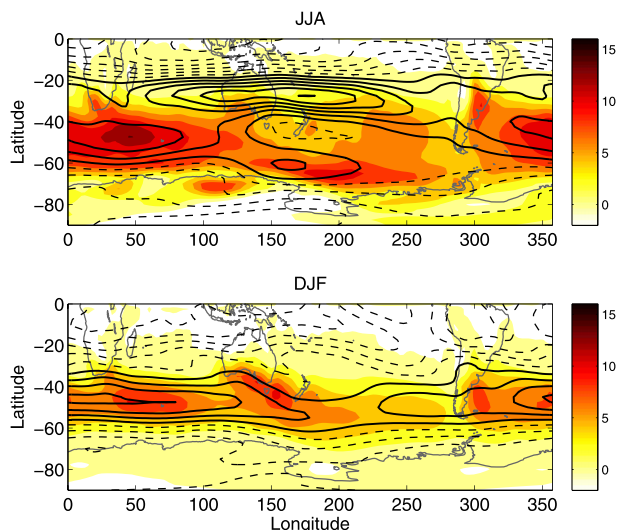
FIG. 9. Climatology of the zonal wind at 300 hPa (contours) and synoptic-eddy poleward heat flux at 850 hPa (shading, m s^{-1} K) as a function of longitude and latitude for the SH (top) winter (JJA) and (bottom) summer (DJF), based on the NCEP–NCAR reanalysis data for years 1969–2011. Dashed contours mark values of 15 m s^{-1} and less and solid contours are for values of 20 m s^{-1} and more, with a contour interval of 5 m s^{-1}.

with summer is partly due to the equatorward shift in the latitude of the Hadley cell edge, and not only due to the intensification of the Hadley circulation. When the subtropical jet is located more equatorward, where the β effect is strong, then baroclinic waves are less able to grow near the jet and transfer its momentum poleward.

6. Summary

This paper studies the maintenance of two flow regimes that are often observed in the atmosphere and the transition between them. In one regime, which we refer to as a "subtropical jet regime" the maximum of the upper-tropospheric zonal mean zonal wind is located at the subtropical edge of the Hadley cell and in the other regime, which we call a "merged jet regime," the maximum of the wind lies inside the Ferrel cell and the jet is created by a merging of the subtropical and eddy-driven jets. The subtropical jet regime is dominated by thermal driving, while in the merged jet regime, convergence of eddy momentum flux also plays a major role. The paper focuses on the questions of how can a subtropical jet be maintained at the edge of the Hadley cell in the presence of eddies and what determines whether eddies will be able to displace the jet poleward and induce a transition to a merged jet regime.

The regime transition is studied using a two-layer modified quasigeostrophic spherical model. The dynamical processes explicitly represented in the model include

baroclinic and barotropic interactions between the waves and the zonal mean flow, advection of zonal mean momentum by the MMC, nonlinear wave–wave interactions, radiative damping, and surface friction.

The maintenance of the merged jet regime in our model is similar to that of the self-maintaining jet described by Robinson (2006): Waves grow baroclinically close to the latitude of the jet, and decay barotropically near the upper-layer critical latitudes at the flanks of the jet, transferring momentum into the jet and maintaining it against the Coriolis force. Surface friction limits the intensity of the surface westerlies and restores the baroclinicity, allowing the waves to keep growing and to maintain the jet.

The maintenance of the subtropical jet regime is mainly by a balance between the advection of momentum by the MMC and the Coriolis force. This balance keeps the maximum of the jet near the subtropical edge of the Hadley cell (Held and Hou 1980). Although the subtropical jet has a strong vertical shear, waves in this regime are relatively weak and grow far poleward of the jet latitude so that their momentum flux near the jet maximum is not strong enough to shift the jet into the Ferrel cell. It was found that what prevents the waves from growing efficiently near the latitude of the jet is the structure of the mean PV gradient: Baroclinic waves tend to be concentrated where the PV gradient is positive and strong at the upper level and negative and strong at the lower level. Since the β effect contributes to a positive PV gradient at both levels, with a stronger effect at low latitudes, it creates an area with positive PV gradient at the lower-layer tropics and subtropics (equatorward of 25°). As a result, the lower-layer wave is confined to higher latitudes, while the upper-layer wave amplitude is concentrated near the jet core, where the PV gradient is strong. When the jet is subtropical, its core is located equatorward of the region of the lower-level negative PV gradient, and this causes a meridional tilt of the wave amplitude with height that reduces the baroclinic growth and confines it to higher latitudes.

It was further shown that the existence of two distinct regimes is related to the fact that certain wave modes grow efficiently in one regime, while different modes dominate the spectrum in the other regime, depending on the configuration of the mean flow: In the merged jet regime, the dominant modes are intermediate scale modes (wavenumbers 4–6) with high phase speeds (between 10 and 20 m s^{-1} in the midlatitudes), which transfer momentum mainly from the subtropics to the midlatitudes, with a weaker flux from high latitudes to the midlatitudes. In the subtropical jet regime, waves comprise two main types of modes: intermediate-scale waves with relatively low phase speeds (between 5 and 10 m s^{-1}

in the midlatitudes) that grow baroclinically at the mid-latitudes and long waves (wavenumbers 1–3) with low or negative (westward) phase speeds that grow baroclini-cally at high latitudes and are confined to the latitudes where the surface winds are easterly. The intermediate-scale waves in the subtropical jet regime transfer mo-mentum mainly from high latitudes to the midlatitudes, with a weaker flux from the subtropics to the midlatitudes. The long waves transfer momentum from around 70° to 60°S.

The transition between the two regimes is abrupt as certain parameters of the model are gradually varied. The abruptness of the transition, together with the above analysis, suggest that the following feedback mechanism takes place: As the wave amplitude is reduced and cor-respondingly the eddy momentum flux is weakened, the effect of thermal forcing from the tropics becomes more dominant than the eddy driving, and the jet shifts equa-torward closer to the edge of the Hadley cell. The equa-torward shift of the jet reduces the efficiency of the baroclinic growth, since the wave structure becomes meridionally tilted with height, as explained above for the subtropical jet regime. The wave amplitude then becomes even weaker, until the waves are unable to maintain the jet inside the Ferrel cell, and the equatorward shift con-tinues until the jet settles at the edge of the Hadley cell, where it is maintained by a balance between the advec-tion of momentum by the MMC and the Coriolis force. The transition may be induced by parameters controlling the wave amplitude directly, as the static stability, ex-pressed by the parameter H in our model; a wave damping parameter, as the parameter r in our model; or by para-meters affecting the wave amplitude indirectly, as the parameter D in our model, which controls the intensity of the tropical heating. As the tropical heating is increased, the Hadley circulation becomes stronger, intensifying the subtropical jet, and increasing its instability until the waves become strong enough to induce a transition to a merged jet regime.

A comparison of the properties of the waves in each regime in the model with those in the atmosphere, as documented by observational studies in the literature (Randel and Held 1991; Kim and Lee 2004), shows a qualitative similarity in the structure of the wave fluxes and their wavenumber and phase speed spectra. It is therefore reasonable to assume that while this model is highly idealized, it does capture the basic mechanisms allowing for each type of jet to be maintained in the atmosphere. However, the transition that was found in the model from a subtropical jet to a merged jet regime as the tropical heating is increased is not supported by zonal mean observations. A closer look at the longitudi-nal structure of the climatological jets in the atmosphere

and a comparison with numerical and observational studies with zonally asymmetric conditions (Williams et al. 2007; Brayshaw et al. 2008) suggests that the zonal localization of the tropical heating in the atmosphere allows the subtropical jet to be maintained in a limited longitudinal sector, while zonally symmetric conditions would have led to a transition to a merged jet regime. This possibility requires further investigation.

APPENDIX A

Model Equations

The equations are based on the QG assumptions for a sphere, with an extra ageostrophic term, representing the advection of zonal mean momentum by the MMC. Our purpose was to get a qualitative representation of the mean-flow momentum balance on one hand and a qualitative representation of the wave–mean flow inter-actions on the other hand, while retaining the simplicity of the QG framework. We found that the best way to do so is to have separate equations for the waves and the mean flow based on slightly different assumptions: first, the ageostrophic term was not added for the waves, and second, the equations for the waves and the mean flow are two different versions of the spherical QG equa-tions, as explained below. The equations are formulated to ensure total energy conservation, while potential ens-trophy is only approximately conserved, as shown in appendix B.

The basic QG assumptions for spherical coordinates lead to nonconservation of energy and potential ens-trophy (Mak 1991) unless further approximations are made. One common approximation that conserves en-ergy and potential enstrophy was developed in Pedlosky [1987, his Eq. (6.5.21)] and used, for example, in Marshall and Molteni (1993). This approximation leads to a PV conservation equation on a sphere ($dq/dt = 0$), where the PV is defined with a constant Coriolis parameter in the stretching term but with the full variation of the Coriolis parameter in the planetary vorticity term. A more gen-eral version of Pedlosky's approximation includes the full

variation of the Coriolis parameter in the stretching term. This version, which also conserves energy and potential enstrophy, was first developed by Charney and Stern (1962) and used in many other studies (e.g., Hollingsworth et al. 1976; Plumb 1986; Schubert et al. 2009). We have chosen to use Charney and Stern's approximation for the waves [Eq.(3)], since we found the assumption of a constant Coriolis parameter in the stretching term too crude for a model used to study properties of the general circulation. In this approximation, the PV is defined as follows:

$$q \equiv 2\Omega\mu + \nabla^2\psi + \left(\frac{2\Omega\mu}{N}\right)^2\frac{\partial^2\psi}{\partial z^2}, \qquad \text{(A1)}$$

where N is the Brunt–Väisälä frequency and ψ is the streamfunction. This approximation is based on two assumptions: 1) The geostrophic part of the flow is approximated by a nondivergent flow that is derived from a streamfunction defined as $\psi \equiv \Phi/f$, where Φ is the geopotential and $f = 2\Omega\mu$ is the full latitudinally dependent Coriolis parameter. 2) The advection of planetary vorticity by the ageostrophic flow [$(V_a)(\partial f/\partial\mu)$] is neglected in the vorticity equation. Both of these assumptions are valid if the flow variables vary in latitude much faster than the Coriolis parameter (Charney and Stern 1962), which may be a good approximation far enough from the tropics, where most of the eddy activity occurs.

For the mean flow there was no need to assume $\psi \equiv \Phi/f$, since for a purely zonal flow the geostrophic part of the flow is nondivergent without any further assumptions. Therefore, $\overline{U_g}$ in Eq. (2) was derived instead from the true geostrophic relations $\partial\overline{\psi}/\partial\mu \equiv (1/f)(\partial\overline{\Phi}/\partial\mu)$, where $\overline{U_g} = -[(1 - \mu^2)/a](\partial\overline{\psi}/\partial\mu)$. It turns out that if the true geostrophic relations are used, then the advection of planetary vorticity by the ageostrophic flow should be retained in order to get energy conservation (Lorenz 1960). Furthermore, neglecting it would be equivalent to adding an unrealistic term to the zonal momentum equation. Therefore, both assumptions used for the wave equations were not used for the mean flow.

The use of different assumptions for the mean flow and the waves is not very problematic since the difference is nonnegligible only at the tropics, where there is very little eddy activity, and since we made sure that the total flow field conserves energy in the absence of the nonconservative diabatic and friction terms, as shown in appendix B.

a. Continuous equations

Let us write the equations for a continuous vertical log-pressure coordinate z before discretizing it to two layers. The mean-flow momentum equation [see Eq. (2)]

is given in section 2. The mean-flow heat equation, thermal wind relations, and continuity of the MMC are the QG equations with an extra term for the ageostrophic advection of buoyancy, which cancels for the two-layer model, as shown in section Ab:

$$\frac{\partial\overline{b}}{\partial t} = -N^2\overline{w_a} - \frac{1}{a}\frac{\partial\overline{b}}{\partial\mu}\overline{V_a} - \frac{1}{a}\frac{\partial\overline{(V'_g b')}}{\partial\mu} - \frac{(\overline{b} - \overline{b_E})}{\tau_r}, \qquad \text{(A2)}$$

$$-\frac{(1 - \mu^2)}{a}\frac{\partial\overline{b}}{\partial\mu} = 2\Omega\mu\frac{\partial\overline{U_g}}{\partial z}, \quad \text{and} \qquad \text{(A3)}$$

$$\frac{1}{a}\frac{\partial\overline{V_a}}{\partial\mu} + \frac{\partial\overline{w_a}}{\partial z} = 0, \qquad \text{(A4)}$$

where $b \equiv \partial\Phi/\partial z$ is the buoyancy, b_E is the radiative equilibrium profile of the buoyancy, and τ_r is the radiative relaxation time scale.

Equations (A3) and (A4) may be substituted into Eqs. (2) and (A2) to eliminate $\overline{b}$ and $\overline{w_a}$ from the equations and to obtain a diagnostic equation for $\overline{V_a}$. This will be shown in section Ab for the two-layer equations.

The wave PV equation [Eq. (3)] is given in section 2. The PV q' is defined by the perturbation from the zonal mean of Eq. (A1). The wave wind components and buoyancy are derived from the streamfunction:

$$U'_g = -\left(\frac{1 - \mu^2}{a}\right)\frac{\partial\psi'}{\partial\mu}, \qquad \text{(A5a)}$$

$$V'_g = \frac{1}{a}\frac{\partial\psi'}{\partial\lambda}, \quad \text{and} \qquad \text{(A5b)}$$

$$b' = 2\Omega\mu\frac{\partial\psi'}{\partial z}. \qquad \text{(A5c)}$$

The mean PV $\overline{q}$ in Eq. (3) was approximated according to the constraint of energy conservation—that is, that the change in the total energy of the mean flow due to its interaction with the waves would be equal to minus the change in the total energy of the waves due to their interaction with the mean flow. The QG approximation of Ertel's PV, without any further assumptions, gives $\overline{q} = 2\Omega\mu + \overline{\zeta} + (2\Omega\mu/N^2)(\partial\overline{b}/\partial z)$, where $\overline{\zeta}$ is the mean vorticity. However, energy conservation requires (see section Ba)

$$\frac{\partial\overline{q}}{\partial\mu} \equiv 2\Omega + \frac{\partial\overline{\zeta}}{\partial\mu} + \frac{2\Omega\mu}{N^2}\frac{\partial}{\partial\mu}\left(\frac{\partial\overline{b}}{\partial z}\right), \qquad \text{(A6)}$$

where the meridional derivative ($\partial/\partial\mu$) of the Coriolis parameter in the stretching term, $(2\Omega/N^2)(\partial\overline{b}/\partial z)$, was neglected. Apart from making sure that energy is conserved, this approximation is consistent with the QG

theory assumption that the horizontal variations of the stratification are small, which means that $\partial \overline{b}/\partial z \ll N^2$ [Eq. (5.23) of Vallis (2006)], so that the neglected term is much smaller than the first term on the rhs. Equation (A6) defines only the meridional derivative of $\overline{q}$, but since it never appears in the equations without the derivative, there was no need to determine the constant of integration.

b. Two-layer equations

The vertical coordinate z is discretized to two layers, representing the lower and upper troposphere. We assume no topography at the surface and a rigid lid at the top. The thickness of both layers H is the same and does not vary horizontally. The upper- and lower-layer terms are denoted by the subscripts 1 and 2, respectively. We denote by subscripts M and T the barotropic and baroclinic components of all variables, defined as half the sum and half the difference between the two layer, respectively, so that $P_M \equiv (1/2)(P_1 + P_2)$ and $P_T \equiv (1/2)(P_1 - P_2)$ for any arbitrary variable P.

The model equations may be decomposed to their barotropic and baroclinic components, making use of the fact that for any two arbitrary variables P and Q, $(PQ)_M = P_M Q_M + P_T Q_T$ and $(PQ)_T = P_M Q_T + P_T Q_M$. The vertical derivatives of all the flow variables are assumed to be zero above the upper layer and below the lower layer, so that the second vertical derivatives of the baroclinic and barotropic components become $(\partial^2 P/\partial z^2)_T = -(2/H^2)(P_T)$ and $(\partial^2 P/\partial z^2)_M = 0$. In addition we note that b and w_a are defined at the middle between the two layers and are assumed to be zero at the boundaries, so that $(\partial w_a/\partial z)_1 = -(\partial w_a/\partial z)_2$. Continuity then gives $(V_a)_1 = -(V_a)_2$, or equivalently $(V_a)_M = 0$. From now on, subscripts g are removed and any flow variable without subscript describes the geostrophic part of the flow.

The barotropic and baroclinic components of Eq. (2), with additional numerical diffusion terms, are

$$\frac{\partial \overline{U_M}}{\partial t} = -\frac{1}{a}\frac{\partial}{\partial \mu}[\overline{U_T(V_a)_T}] - \frac{1}{a}\frac{\partial(\overline{U'V'})_M}{\partial \mu}$$
$$- \frac{(\overline{U_M} - \overline{U_T})}{2\tau_f} - \nu \frac{\partial^4 \overline{U_M}}{\partial \mu^4} \quad \text{and} \quad \text{(A7a)}$$

$$\frac{\partial \overline{U_T}}{\partial t} = \left(2\Omega\mu - \frac{1}{a}\frac{\partial \overline{U_M}}{\partial \mu}\right)(\overline{V_a})_T - \frac{1}{a}\frac{\partial(\overline{U'V'})_T}{\partial \mu}$$
$$+ \frac{(\overline{U_M} - \overline{U_T})}{2\tau_f} - \nu \frac{\partial^4 \overline{U_T}}{\partial \mu^4}, \quad \text{(A7b)}$$

where ν is the numerical diffusion coefficient. We used the baroclinic component of the continuity equation [Eq. (A4)] to eliminate $\overline{w_a}$ from the equations.

The baroclinic component of the vertical derivative of the heat equation [see Eq. (A2)] is

$$-\frac{2}{H^2}\frac{\partial \overline{\Phi_T}}{\partial t} = \frac{N^2}{a}\frac{\partial(\overline{V_a})_T}{\partial \mu}$$
$$+ \frac{2}{aH^2}\left[\frac{\partial \overline{\Phi_T}}{\partial \mu}(\overline{V_a})_M + \frac{\partial \overline{\Phi_M}}{\partial \mu}(\overline{V_a})_T\right]$$
$$+ \frac{4\Omega}{aH^2}\frac{\partial(\mu \overline{V'_M \psi'_T})}{\partial \mu} + \frac{2}{\tau_r H^2}[\overline{\Phi_T} - (\overline{\Phi_E})_T].$$
$$\text{(A8)}$$

The second term on the rhs vanishes, because under the assumptions of the two-layer model, $\overline{\Phi_M} = 0$ and $(\overline{V_a})_M = 0$. To get a diagnostic equation for $(\overline{V_a})_T$, we apply the operator $-[H^2(1-\mu^2)/4a\Omega^2](\partial/\partial\mu)$ on Eq. (A8) and add it to Eq. (A7b) multiplied by μ/Ω, making use of the baroclinic component of Eqs. (A3) and (A4):

$$-\frac{2(1-\mu^2)}{\epsilon}\frac{\partial^2(\overline{V_a})_T}{\partial\mu^2} + \left(2\mu^2 - \frac{\mu}{a\Omega}\frac{\partial \overline{U_M}}{\partial\mu}\right)(\overline{V_a})_T$$
$$= \frac{(1-\mu^2)}{a^2\Omega}\frac{\partial^2}{\partial\mu^2}(\mu \overline{V'_M \psi'_T}) + \frac{\mu}{a\Omega}\frac{\partial(\overline{U'V'})_T}{\partial\mu}$$
$$- \frac{\mu}{2\Omega\tau_f}(\overline{U_M} - \overline{U_T}) + \frac{\mu}{\Omega\tau_r}[(\overline{U_T})_E - \overline{U_T}], \quad \text{(A9)}$$

where $\epsilon \equiv 8(a\Omega/NH)^2$, and $(\overline{U_T})_E$ is the radiative equilibrium profile of the thermal wind.

The wave equation [see Eq. (3)] and the perturbation from zonal average of Eq. (A1) are also decomposed to barotropic and baroclinic components, with additional numerical diffusion terms:

$$\frac{\partial q'_M}{\partial t} = -\frac{\overline{U_M}}{a(1-\mu^2)}\frac{\partial q'_M}{\partial\lambda} - \frac{\overline{U_T}}{a(1-\mu^2)}\frac{\partial q'_T}{\partial\lambda} - \frac{V'_M}{a}\frac{\partial \overline{q}_M}{\partial\mu} - \frac{V'_T}{a}\frac{\partial \overline{q}_T}{\partial\mu} - \left[\frac{U'_M}{a(1-\mu^2)}\frac{\partial q'_M}{\partial\lambda}\right]' - \left[\frac{U'_T}{a(1-\mu^2)}\frac{\partial q'_T}{\partial\lambda}\right]'$$
$$- \left(\frac{V'_M}{a}\frac{\partial q'_M}{\partial\mu}\right)' - \left(\frac{V'_T}{a}\frac{\partial q'_T}{\partial\mu}\right)' - \frac{\nabla^2(\psi'_M - \psi'_T)}{2\tau_f} - \nu\nabla^4(q'_M), \quad \text{(A10a)}$$

$$\frac{\partial q'_T}{\partial t} = -\frac{\overline{U_M}}{a(1-\mu^2)}\frac{\partial q'_T}{\partial \lambda} - \frac{\overline{U_T}}{a(1-\mu^2)}\frac{\partial q'_M}{\partial \lambda} - \frac{V'_M}{a}\frac{\partial \overline{q}_T}{\partial \mu} - \frac{V'_T}{a}\frac{\partial \overline{q}_M}{\partial \mu} - \left[\frac{U'_M}{a(1-\mu^2)}\frac{\partial q'_T}{\partial \lambda}\right]' - \left[\frac{U'_T}{a(1-\mu^2)}\frac{\partial q'_M}{\partial \lambda}\right]'$$

$$-\left(\frac{V'_M}{a}\frac{\partial q'_T}{\partial \mu}\right)' - \left(\frac{V'_T}{a}\frac{\partial q'_M}{\partial \mu}\right)' + \frac{\nabla^2(\psi'_M - \psi'_T)}{2\tau_f} + \frac{\epsilon\mu^2}{a^2\tau_r}\psi'_T - \nu\nabla^4(q'_T), \tag{A10b}$$

$$q'_M = \nabla^2\psi'_M, \quad \text{and} \tag{A11a}$$

$$q'_T = \nabla^2\psi'_T - \frac{\epsilon}{a^2}\mu^2\psi'_T. \tag{A11b}$$

The components of the mean PV gradient, $\partial\overline{q}_M/\partial\mu$ and $\partial\overline{q}_T/\partial\mu$, which appear in Eqs. (A10a) and (A10b), are calculated by taking the two-layer version of Eq. (A6):

$$\frac{1}{a}\frac{\partial\overline{q}_M}{\partial\mu} = \frac{2\Omega}{a} - \frac{1}{a^2}\frac{\partial^2\overline{U_M}}{\partial\mu^2} \quad \text{and} \tag{A12a}$$

$$\frac{1}{a}\frac{\partial\overline{q}_T}{\partial\mu} = -\frac{1}{a^2}\frac{\partial^2\overline{U_T}}{\partial\mu^2} + \frac{\epsilon}{a^2}\left(\frac{\mu^2}{1-\mu^2}\right)\overline{U_T}. \tag{A12b}$$

Equations (A7a), (A7b), (A10a), and (A10b) are integrated in time using the Adams–Bashforth scheme. We use the spectral transform method with a horizontal resolution of T42. Each time step $(\overline{V_a})_T$ is calculated

from Eq. (A9), and the wind components of the wave are derived from the streamfunctions ψ'_M and ψ'_T, which are calculated by inverting Eqs. (A11a) and (A11b). Both equations were inverted in spectral space, which is straightforward for Eq. (A11a), while for Eq. (A11b) we used a method developed by Verkley (2009), which takes advantage of the special properties of the Legendre functions.

c. Equations for the integrations of set D

For the set of integrations with additional diabatic heating at the tropics (set D in Table 1), another term was added to Eq. (A9):

$$-\frac{2(1-\mu^2)}{\epsilon}\frac{\partial^2(\overline{V_a})_T}{\partial\mu^2} + \left(2\mu^2 - \frac{\mu}{a\Omega}\frac{\partial\overline{U_M}}{\partial\mu}\right)(\overline{V_a})_T = \frac{(1-\mu^2)}{a^2\Omega}\frac{\partial^2}{\partial\mu^2}(\mu\overline{V'_M\psi'_T}) + \frac{\mu}{a\Omega}\frac{\partial(\overline{U'V'})_T}{\partial\mu}$$

$$-\frac{\mu}{2\Omega\tau_f}(\overline{U_M} - \overline{U_T}) + \frac{\mu}{\Omega\tau_r}[(\overline{U_T})_E - \overline{U_T}] - \frac{2aD}{\epsilon HN^2}(1-\mu^2)\frac{\partial Q}{\partial\mu}, \tag{A13}$$

where D is the diabatic heating parameter, $Q = Q_0 \exp\{-[(\phi-\phi_0)/\sigma]^2\}$ is the diabatic heating profile, $Q_0 = 10^{-6}\,\text{m\,s}^{-3}$, $\phi_0 = 10°$, and $\sigma = 5°$.

In addition, a tropical vertical mixing term for the zonal wind was added to Eq. (A7b) to prevent a transition to a state with superrotation (e.g., Kraucunas and Hartmann 2005), which would otherwise occur in the presence of strong tropical diabatic heating. The intensity of the vertical mixing is proportional to the diabatic heating parameter D and was chosen to have the minimal value needed to suppress superrotation:

$$\frac{\partial\overline{U_T}}{\partial t} = \left(2\Omega\mu - \frac{1}{a}\frac{\partial\overline{U_M}}{\partial\mu}\right)(\overline{V_a})_T - \frac{1}{a}\frac{\partial(\overline{U'V'})_T}{\partial\mu}$$

$$+ \frac{(\overline{U_M} - \overline{U_T})}{2\tau_f} - \nu\frac{\partial^4\overline{U_T}}{\partial\mu^4} - VM\overline{U_T}, \tag{A14}$$

where $VM = DVM_0\exp[-(\phi/10°)^2]$ and $VM_0 = 10^{-5}\,\text{s}^{-1}$.

APPENDIX B

Energy and Potential Enstrophy Balance

a. Energy conservation

The total energy is the sum of the kinetic energy (KE) and the available potential energy (APE) of the mean flow and the waves:

$$\langle\text{KE}_{\text{MF}}\rangle \equiv \left\langle\frac{1}{2}(\overline{u})^2\right\rangle,$$

$$\langle\text{APE}_{\text{MF}}\rangle \equiv \left\langle\frac{1}{2N^2}(\overline{b})^2\right\rangle,$$

$$\langle\text{KE}_{\text{WV}}\rangle \equiv \left\langle\frac{1}{2}[(u')^2 + (v')^2]\right\rangle = -\left\langle\frac{1}{2}(\psi'\zeta')\right\rangle,$$

$$\langle\text{APE}_{\text{WV}}\rangle \equiv \left\langle\frac{1}{2N^2}(b')^2\right\rangle = \left\langle\frac{1}{2}[(\zeta' - q')\psi']\right\rangle, \tag{B1}$$

where angle brackets denote spatial average and subscripts MF and WV denote mean flow and waves, respectively.

The model equations conserve the total energy in the absence of the nonconserving terms of radiative damping, surface friction, and numerical diffusion. This can be proved by showing that the total energy tendency is zero:

$$\left\langle \frac{\partial}{\partial t}(\text{KE}_{\text{MF}} + \text{APE}_{\text{MF}} + \text{KE}_{\text{WV}} + \text{APE}_{\text{WV}}) \right\rangle = 0.$$

The individual time tendency terms are obtained by standard manipulation of Eqs. (A7a), (A7b), (A2), (A10a), and (A10b). When doing this, one finds that all the conversion terms—between KE_{MF} and APE_{MF}, between KE_{WV} and APE_{WV}, between KE_{MF} and KE_{WV}, and between APE_{MF} and APE_{WV}—cancel each other. The conversion of APE_{WV} to APE_{MF} depends on the definition of $\overline{q_T}$, which does not appear explicitly in the mean-flow equations. For this term to cancel the conversion of APE_{MF} to APE_{WV}, $\overline{q_T}$ has to be defined according to Eq. (A12b), which is the baroclinic component of Eq. (A6), as discussed in section Aa.

The degree of energy conservation was also evaluated numerically from the model integrations presented in this paper. It was found that most of the time dependence of the total energy is due to the nonconserving model terms, meaning that without them energy would have been close to conservation. For example, in the model integration with $H = 9$ km from set H (see Table 1), during the first 20 days of the integration, when the system is far from steady state, the time-averaged time derivative of the total energy is $(dE/dt)_{\text{avg}} = 3.1 \times 10^{-5}$ m^2 s^{-3}, while the time-averaged time derivative of energy due to nonconserving terms is $(dE_{\text{nc}}/dt)_{\text{avg}} = 3.2 \times 10^{-5}$ m^2 s^{-3}, leaving a residual of $(dE/dt - dE_{\text{nc}}/dt)_{\text{avg}} = -0.1 \times 10^{-5}$ m^2 s^{-3} of nonconservation due to numerical errors, which is 3% of the total energy time derivative. During days 20–1500, the system is close to statistically steady state and the total energy time derivative fluctuates around zero, with $(dE/dt)_{\text{avg}} = 0.021 \times 10^{-5}$ m^2 s^{-3}, and a standard deviation $(dE/dt)_{\text{std}} = 0.88 \times 10^{-5}$ m^2 s^{-3}. This essentially statistically steady state is enabled by a balance between energy generation by the radiative relaxation of the mean flow, which is $(dE_{\text{rad}}/dt)_{\text{avg}} = 5.4 \times 10^{-5}$ m^2 s^{-3}, and all other nonconserving terms of surface friction, radiative damping of the waves, and numerical diffusion, which act as energy sinks. The small residual decay of energy, calculated by subtracting the time average of the energy tendency due to the nonconserving terms from the time average of the total energy tendency, of about $(dE/dt - dE_{\text{nc}}/dt)_{\text{avg}} = -0.28 \times 10^{-5}$ m^2 s^{-3}, which is 5.2% of the radiative relaxation term, is attributed to the numerical error. It should be noted that part of this numerical imbalance could be due to errors in the calculation of the mean-flow radiative relaxation term, which involves two latitudinal integrations, so that errors in the model integration itself may be much smaller.

b. Potential enstrophy balance

Potential enstrophy S is defined as half the square of the potential vorticity:

$$\langle S \rangle = \langle S_{\text{MF}} \rangle + \langle S_{\text{WV}} \rangle \equiv \left\langle \frac{1}{2}(\overline{q})^2 \right\rangle + \left\langle \frac{1}{2}(q')^2 \right\rangle$$

As explained in appendix A, the assumptions that were used for the wave equations lead to a PV conservation equation, $dq/dt = 0$, in the absence of dissipation terms and, hence, to potential enstrophy conservation. However, the assumptions used for the mean flow do not lead to a PV conservation equation. Instead, the conserved quantity under these assumptions is $\overline{q_M} + \widetilde{\overline{q_T}} + (\overline{U_T}/a\mu)$ [see Eq. (2.19) of Mak (1991) with $\mathbf{V}_2 \cdot V_g = 0$], where $\widetilde{\overline{q_T}} = \overline{\zeta_T} + (2\Omega\mu/N^2)(\partial \overline{b}/\partial z)_T$, which is slightly different from $\overline{q_T}$, defined in Eq. (A6).

In the numerical integrations, this nonconservation of potential enstrophy by the model equations creates a nonnegligible sink of potential enstrophy, which is roughly a quarter of the total enstrophy source terms. The model enstrophy does, however, reach a statistically steady state within a relatively short time, suggesting the flow arranges itself so that the source terms balance this built-in enstrophy loss. For example, in the model integration with $H = 9$ km from set H, during the statistically steady state period, when $(dS/dt)_{\text{avg}} = 0.04 \times 10^{-16}$ s^{-3} and $(dS/dt)_{\text{std}} = 2 \times 10^{-16}$ s^{-3}, the time averages of the nonconserving terms show that both mean-flow radiative damping and surface friction are sources of potential enstrophy, with $[(dS_{\text{rad}})_{\text{MF}}/dt]_{\text{avg}} = 6.9 \times 10^{-16}$ s^{-3} and $[(dS_{\text{fric}})_{\text{MF}}/dt]_{\text{avg}} = 1.3 \times 10^{-16}$ s^{-3}, while numerical diffusion and wave radiative damping and surface friction are sinks of potential enstrophy, with $[(dS_{\text{rad}})_{\text{WV}}/dt]_{\text{avg}} = -1.6 \times 10^{-16}$ s^{-3}, $[(dS_{\text{fric}})_{\text{WV}}/dt]_{\text{avg}} = -0.9 \times 10^{-16}$ s^{-3}, and $(dS_{\text{diff}}/dt)_{\text{avg}} = -3.3 \times 10^{-16}$ s^{-3}, so that the built-in enstrophy mismatch accounts for a loss of $(dS/dt)_{\text{avg}} - (dS_{\text{nc}}/dt)_{\text{avg}} = -2.3 \times 10^{-16}$, which is 28% of the sum of the source terms.

REFERENCES

Brayshaw, D. J., B. Hoskins, and M. Blackburn, 2008: The storm-track response to idealized SST perturbations in an aqua-planet GCM. *J. Atmos. Sci.,* **65,** 2842–2860.

Chang, E. K. M., 1995: The influence of Hadley circulation intensity changes on extratropical climate in an idealized model. *J. Atmos. Sci.,* **52,** 2006–2024.

Charney, J. G., and M. E. Stern, 1962: On the stability of internal baroclinic jet in a rotating atmosphere. *J. Atmos. Sci.,* **19,** 159–172.

Dima, I. M., J. M. Wallace, and I. Kraucunas, 2005: Tropical zonal momentum balance in the NCEP reanalyses. *J. Atmos. Sci.,* **62,** 2499–2513.

Eichelberger, S. J., and D. L. Hartmann, 2007: Zonal jet structure and the leading mode of variability. *J. Climate,* **20,** 5149–5163.

Fjørtoft, R., 1950: Application of integral theorems in deriving criteria of stability for laminar flows and for the baroclinic circular vortex. Geofysiske Publ. 17, 52 pp.

Gerber, E. P., and G. K. Vallis, 2007: Eddy–zonal flow interactions and the persistence of the zonal index. *J. Atmos. Sci.,* **64,** 3296–3311.

Heifetz, E., C. H. Bishop, B. J. Hoskins, and J. Methven, 2004: The counter-propagating Rossby-wave perspective on baroclinic instability. I: Mathematical basis. *Quart. J. Roy. Meteor. Soc.,* **130,** 211–231.

Held, I. M., and A. Y. Hou, 1980: Nonlinear axially symmetric circulations in a nearly inviscid atmosphere. *J. Atmos. Sci.,* **37,** 515–533.

Hollingsworth, A., A. J. Simmons, and B. J. Hoskins, 1976: The effect of spherical geometry on momentum transports in simple baroclinic flows. *Quart. J. Roy. Meteor. Soc.,* **102,** 901–911.

Kim, H. K., and S. Lee, 2004: The wave–zonal mean flow interaction in the Southern Hemisphere. *J. Atmos. Sci.,* **61,** 1055–1067.

Korty, R. L., and T. Schneider, 2008: Extent of Hadley circulations in dry atmospheres. *Geophys. Res. Lett.,* **35,** L23803, doi:10.1029/2008GL035847.

Kraucunas, I., and D. L. Hartmann, 2005: Equatorial superrotation and the factors controlling the zonal-mean zonal winds in the tropical upper troposphere. *J. Atmos. Sci.,* **62,** 371–389.

Kushnir, Y., 1987: Retrograding wintertime low-frequency disturbances over the North Pacific Ocean. *J. Atmos. Sci.,* **44,** 2727–2742.

Lee, S., and H. K. Kim, 2003: The dynamical relationship between subtropical and eddy-driven jets. *J. Atmos. Sci.,* **60,** 1490–1503.

Lindzen, R. S., and A. Y. Hou, 1988: Hadley circulations for zonally averaged heating centered off the equator. *J. Atmos. Sci.,* **45,** 2416–2427.

Lorenz, E. N., 1960: Energy and numerical weather prediction. *Tellus,* **12,** 364–373.

Lu, J., G. Chen, and D. M. W. Frierson, 2010: The position of the midlatitude storm track and eddy-driven westerlies in aquaplanet AGCMs. *J. Atmos. Sci.,* **67,** 3984–4000.

Mak, M., 1991: Influences of the earth's sphericity in the quasi-geostrophic theory. *J. Meteor. Soc. Japan,* **69,** 497–511.

Marshall, J., and F. Molteni, 1993: Toward a dynamical understanding of planetary-scale flow regimes. *J. Atmos. Sci.,* **50,** 1792–1818.

Mechoso, C. R., and D. L. Hartmann, 1982: An observational study of traveling planetary waves in the Southern Hemisphere. *J. Atmos. Sci.,* **39,** 1921–1935.

Nakamura, H., and T. Sampe, 2002: Trapping of synoptic-scale disturbances into the North-Pacific subtropical jet core in midwinter. *Geophys. Res. Lett.,* **29,** doi:10.1029/2002GL015535.

——, and A. Shimpo, 2004: Seasonal variations in the Southern Hemisphere storm tracks and jet streams as revealed in a reanalysis dataset. *J. Climate,* **17,** 1828–1844.

——, T. Sampe, Y. Tanimoto, and A. Shimpo, 2004: Observed associations among storm tracks, jet streams and midlatitude oceanic fronts. *Earth's Climate: The Ocean-Atmosphere Interaction, Geophys. Monogr.,* Vol. 147, Amer. Geophys. Union, 329–345.

O'Rourke, A. K., and G. K. Vallis, 2013: Jet interaction and the influence of a minimum phase speed bound on the propagation of eddies. *J. Atmos. Sci.,* **70,** 2614–2628.

Panetta, R. L., 1993: Zonal jets in wide baroclinically unstable regions: Persistence and scale selection. *J. Atmos. Sci.,* **50,** 2073–2106.

Pedlosky, J., 1987: *Geophysical Fluid Dynamics.* 2nd ed. Springer-Verlag, 710 pp.

Plumb, R. A., 1986: Three-dimensional propagation of transient quasi-geostrophic eddies and its relationship with the eddy forcing of the time-mean flow. *J. Atmos. Sci.,* **43,** 1657–1678.

Randel, W. J., and I. M. Held, 1991: Phase speed spectra of transient eddy fluxes and critical layer absorption. *J. Atmos. Sci.,* **48,** 688–697.

Robinson, W. A., 2006: On the self-maintenance of midlatitude jets. *J. Atmos. Sci.,* **63,** 2109–2122.

Salmon, R., I. M. Held, J. Fields, and J.-L. Thiffeault, 2001: The general circulation of the atmosphere: 2000 program of study in geophysical fluid dynamics. Woods Hole Oceanographic Institution Tech. Rep. WHOI-2001-03, 179 pp.

Schneider, T., and S. Bordoni, 2008: Eddy-mediated regime transitions in the seasonal cycle of a Hadley circulation and implications for monsoon dynamics. *J. Atmos. Sci.,* **65,** 915–934.

Schubert, W. H., R. K. Taft, and L. G. Silvers, 2009: Shallow water quasi-geostrophic theory on the sphere. *J. Adv. Model. Earth Syst.,* **1** (2), doi:10.3894/JAMES.2009.1.2.

Son, S. W., and S. Lee, 2005: The response of westerly jets to thermal driving in a primitive equation model. *J. Atmos. Sci.,* **62,** 3741–3757.

Vallis, G. K., 2006: *Atmospheric and Oceanic Fluid Dynamics.* Cambridge University Press, 745 pp.

Verkley, W. T. M., 2009: A balanced approximation of the one-layer shallow-water equations on a sphere. *J. Atmos. Sci.,* **66,** 1735–1748.

Walker, C. C., and T. Schneider, 2006: Eddy influences on Hadley circulations: Simulations with an idealized GCM. *J. Atmos. Sci.,* **63,** 3333–3350.

Williams, L. N., S. Lee, and S. W. Son, 2007: Dynamics of the Southern Hemisphere spiral jet. *J. Atmos. Sci.,* **64,** 548–563.